LI
LABORATORY INVESTIGATION
THE BASIC AND TRANSLATIONAL PATHOLOGY RESEARCH JOURNAL
VOLUME 100 | SUPPLEMENT 1 | MARCH 2020

ABSTRACTS

GENERAL SURGICAL PATHOLOGY (833-859)

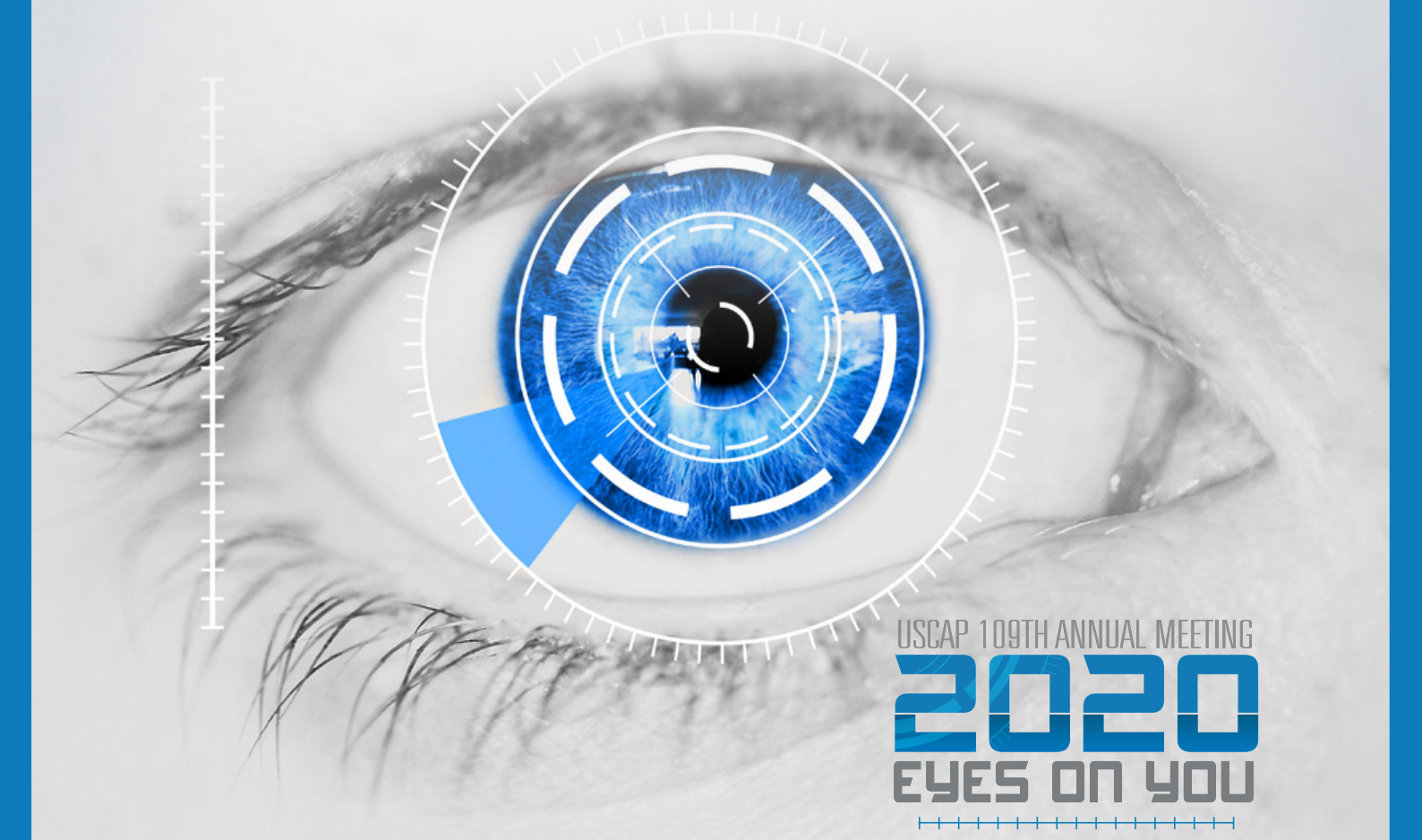

FEBRUARY 29-MARCH 5, 2020

LOS ANGELES CONVENTION CENTER
LOS ANGELES, CALIFORNIA

Published by
SPRINGER NATURE
www.ModernPathology.org

USCAP Creating a Better Pathologist
AN OFFICIAL JOURNAL OF THE UNITED STATES AND CANADIAN ACADEMY OF PATHOLOGY

EDUCATION COMMITTEE

Jason L. Hornick, Chair

Rhonda K. Yantiss, Chair, Abstract Review Board and Assignment Committee

Laura W. Lamps, Chair, CME Subcommittee

Steven D. Billings, Interactive Microscopy Subcommittee

Raja R. Seethala, Short Course Coordinator

Ilan Weinreb, Subcommittee for Unique Live Course Offerings

David B. Kaminsky (Ex-Officio)

Zubair Baloch
Daniel Brat
Ashley M. Cimino-Mathews
James R. Cook
Sarah Dry
William C. Faquin
Yuri Fedoriw
Karen Fritchie
Lakshmi Priya Kunju
Anna Marie Mulligan
Rish K. Pai
David Papke, Pathologist-in-Training
Vinita Parkash
Carlos Parra-Herran
Anil V. Parwani
Rajiv M. Patel
Deepa T. Patil
Lynette M. Sholl
Nicholas A. Zoumberos, Pathologist-in-Training

ABSTRACT REVIEW BOARD

Benjamin Adam
Narasimhan Agaram
Rouba Ali-Fehmi
Ghassan Allo
Isabel Alvarado-Cabrero
Catalina Amador
Roberto Barrios
Rohit Bhargava
Jennifer Boland
Alain Borczuk
Elena Brachtel
Marilyn Bui
Eric Burks
Shelley Caltharp
Barbara Centeno
Joanna Chan
Jennifer Chapman
Hui Chen
Beth Clark
James Conner
Alejandro Contreras
Claudiu Cotta
Jennifer Cotter
Sonika Dahiya
Farbod Darvishian
Jessica Davis
Heather Dawson
Elizabeth Demicco
Katie Dennis
Anand Dighe
Suzanne Dintzis
Michelle Downes
Andrew Evans
Michael Feely
Dennis Firchau
Gregory Fishbein
Andrew Folpe
Larissa Furtado
Billie Fyfe-Kirschner
Giovanna Giannico
Anthony Gill
Paula Ginter
Tamara Giorgadze
Purva Gopal
Anuradha Gopalan
Abha Goyal
Rondell Graham
Alejandro Gru
Nilesh Gupta
Mamta Gupta
Gillian Hale
Suntrea Hammer
Malini Harigopal
Douglas Hartman
John Higgins
Mai Hoang
Mojgan Hosseini
Aaron Huber
Peter Illei
Doina Ivan
Wei Jiang
Vickie Jo
Kirk Jones
Neerja Kambham
Chiah Sui Kao
Dipti Karamchandani
Darcy Kerr
Ashraf Khan
Francesca Khani
Rebecca King
Veronica Klepeis
Gregor Krings
Asangi Kumarapeli
Alvaro Laga
Steven Lagana
Keith Lai
Michael Lee
Cheng-Han Lee
Madelyn Lew
Zaibo Li
Faqian Li
Ying Li
Haiyan Liu
Xiuli Liu
Yen-Chun Liu
Lesley Lomo
Tamara Lotan
Anthony Magliocco
Kruti Maniar
Emily Mason
David McClintock
Bruce McManus
David Meredith
Anne Mills
Neda Moatamed
Sara Monaco
Atis Muehlenbachs
Bita Naini
Dianna Ng
Tony Ng
Michiya Nishino
Scott Owens
Jacqueline Parai
Yan Peng
Manju Prasad
Peter Pytel
Stephen Raab
Joseph Rabban
Stanley Radio
Emad Rakha
Preetha Ramalingam
Priya Rao
Robyn Reed
Michelle Reid
Natasha Rekhtman
Jordan Reynolds
Michael Rivera
Andres Roma
Avi Rosenberg
Esther Rossi
Peter Sadow
Steven Salvatore
Souzan Sanati
Anjali Saqi
Jeanne Shen
Jiaqi Shi
Gabriel Sica
Alexa Siddon
Deepika Sirohi
Kalliopi Siziopikou
Sara Szabo
Julie Teruya-Feldstein
Khin Thway
Rashmi Tondon
Jose Torrealba
Andrew Turk
Evi Vakiani
Christopher VandenBussche
Paul VanderLaan
Olga Weinberg
Sara Wobker
Shaofeng Yan
Anjana Yeldandi
Akihiko Yoshida
Gloria Young
Minghao Zhong
Yaolin Zhou
Hongfa Zhu
Debra Zynger

To cite abstracts in this publication, please use the following format: **Author A, Author B, Author C, et al. Abstract title (abs#). In "File Title."** ***Laboratory Investigation*** **2020; 100 (suppl 1): page#**

833 TTF-1 and Napsin A-Positivity is Rare in Gastroesophageal Adenocarcinomas: An Affirmation

Ibrahim Abukhiran[1], Matthew Gosse[2], Robert Humble[1], Andrew Bellizzi[1]
[1]University of Iowa Hospitals and Clinics, Iowa City, IA, [2]Iowa City, IA

Disclosures: Ibrahim Abukhiran: None; Matthew Gosse: None; Robert Humble: None; Andrew Bellizzi: None

Background: Pathologists rely on TTF-1 and napsin A to establish a pulmonary origin in adenocarcinomas (AdCA) of occult origin. A recent paper reported a shockingly high rate of positivity for these markers in esophageal AdCA: 88% for TTF-1 and 79% for napsin A, though only 24 cases were examined (PMID: 23899066). This result is so discordant from pathologists' anecdotal experience that it has caused some to question the value of immunohistochemistry (IHC) in the workup of the carcinoma of unknown primary (CUP)--along the lines of "everything stains for everything, so why even bother?" In their review of the IHC workup of CUP, Conner and Hornick estimated a rate of TTF-1-positivity in gastroesophageal AdCA of <10% (PMID: 25844674).

Design: We assembled our institutional cohort (1991-2018) of gastroesophageal AdCAs with sufficient material to construct tissue microarrays. All glass slides/pathology reports were reviewed for tumor epicenter (esophagus, GEJ, stomach), Lauren classification, and presence of conspicuous tumor infiltrating lymphocytes (TILs); gender was recorded; TTF-1, napsin A, and MMR IHC was performed, and CDX2 and CDH17 IHC was performed on TTF-1/napsin A-positive cases. Lineage-specific IHC was assessed for intensity (0-3+) and extent (0-100%), and an H-score was calculated. We also visualized *NKX2-1* (gene that encodes TTF-1) and *NAPSA* (napsin A) gene expression in esophageal and lung AdCAs using cBioPortal (cbioportal.org).

Results: We examined 329 samples (223 primaries, 78 lymph node metastases, 23 distant metastases, 5 recurrences) from 249 patients (206M:43W; 64% intestinal [I], 15% diffuse [D], 12% mixed [M], 9% other; 14% with conspicuous TILs; 2.4% MMR-deficient). These included 109 esophageal, 68 gastroesophgeal junction (GEJ), and 72 gastric AdCAs. TTF-1 and/or napsin A-positivity was noted in 12 samples from 9 patients (mean/median H-score of 38/20 for TTF-1, 9/4 for napsin A), representing 4% of esophageal, 1.5% of GEJ, and 6% of gastric AdCAs. 7 samples were also CDX2 and/or CDH17-positive (Figure 1). TTF-1/napsin A-positive cases showed no special features (8M:2W; 6 I, 2 M, 1 D; 17% with conspicuous TILs; all MMR intact). There is little to no overlap in gene expression between esophageal and lung AdCA (Figure 2).

Figure 1 - 833

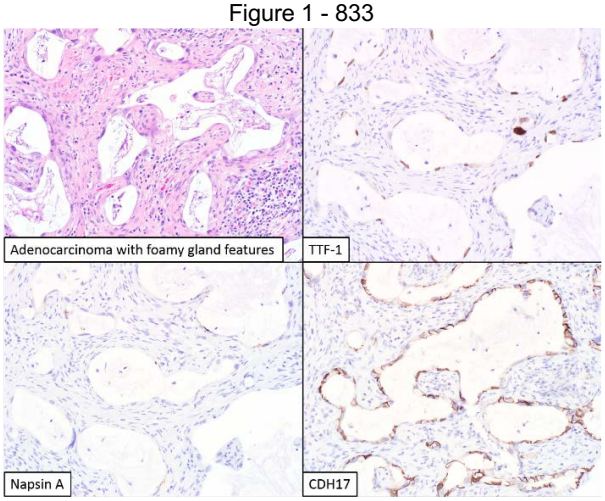

Figure 2 - 833

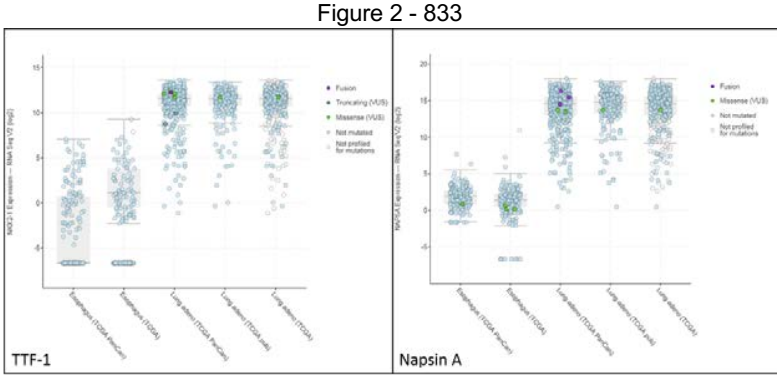

Conclusions: Aberrant expression of lung markers is uncommon in gastroesophageal AdCA, affirming their value in the IHC workup of CUP. Published results discordant with one's clinical experience should be regarded with suspicion.

834 SMARCA4(BRG1) and SMARCB1(INI1) Immunoexpression in TTF1 Negative Neuroendocrine Carcinoma

Fnu Alnoor[1], Jatin Gandhi[1], Jorge Solares[1], Joel Gradowski[2]
[1]University of Tennessee Health Science Center, Memphis, TN, [2]University of Tennessee Health Sciences Center, Germantown, TN

Disclosures: Fnu Alnoor: None; Jatin Gandhi: None; Jorge Solares: None; Joel Gradowski: None

Background: SMARCA4(BRG1) and SMARCB1(INI1) are tumor suppressor genes, subunits of SWI/SNF complex, and their mutations have been implicated in the pathogenesis of many different tumors. Mutations in these genes can be observed as loss of expression by

immunohistochemistry (IHC). The objective of this study was to investigate the loss of expression of BRG1 and INI1 in neuroendocrine carcinomas(NEC), especially in TTF1 negative cases to see if they are analogous to small-cell carcinoma of the ovary, hypercalcemic type (SCCOHT); which in recent years have been proposed to be renamed as 'malignant rhabdoid tumor of the ovary'. The potential role of these tumor suppressor genes in small cell carcinoma (SCC), large cell neuroendocrine carcinoma (LCNEC), and Merkel cell carcinoma (MCC) largely remains unknown.

Design: Cases of previously diagnosed SCC (2016-2019, n=21; pulmonary [n=18] and extra-pulmonary[n=3]), LCNEC (2016-2019, n=17; pulmonary [n=13] and extra-pulmonary[n=4]), and MCC (2013-2019, n=23) from various sites were selected. IHC staining with BRG1 (G-7) and TTF1 (SPT24) was performed on Leica Bond III, and INI1 (MRQ-27) was performed on Ventana platform using paraffin embedded tissue blocks. The expression pattern was interpreted as: retained, hybrid (partial strong and partial negative) and complete loss.

Results: SCC and LCNEC cases were divided as TTF1 positive and TTF1 negative. TTF1 positive SCC n=11, TTF1 positive LCNEC n=6; TTF1 negative SCC n=10, TTF1 negative LCNEC n=11. One case of TTF1 negative SCC (lung) showed hybrid expression of BRG1 while all TTF1 positive SCC showed retained expression of BRG1. All cases of SCC and LCNEC showed retained expression of INI1. Amongst TTF1 negative LCNEC, one case showed complete loss (lung) and one had hybrid expression (lung) of BRG1. BRG1 and INI1 was retained in all cases of MCC. All cases of SCC and LCNEC showed retained expression of INI1.

Conclusions: Loss of BRG1 and/or INI1 has been implicated recently in many tumors. Our study highlights that SMARCA4 is deficient in a subset of NEC and may play an important role in driving these tumors. Inactivation of BRG1 in a subset of TTF1 negative neuroendocrine carcinomas may illuminate a potential role for EZH2 inhibitor targeted therapy in a manner like some preliminary data on SCCOHT. In addition, our study is the first to show that BRG1 and INI1 expression are retained in MCC and hence the biology of MCC might be completely exclusive of these two tumor suppressor genes.

835 Utility of NTRK RNA In Situ Hybridization in NTRK Fusion-Positive Tumors

Baris Boyraz[1], Azfar Neyaz[2], Jason Hornick[3], Ivan Chebib[4], Vikram Deshpande[5]
[1]Massachusettes General Hospital, Boston, MA, [2]Massachusetts General Hospital, Malden, MA, [3]Brigham and Women's Hospital, Harvard Medical School, Boston, MA, [4]Massachusetts General Hospital, Harvard Medical School, Boston, MA, [5]Massachusetts General Hospital, Boston, MA

Disclosures: Baris Boyraz: None; Azfar Neyaz: None; Jason Hornick: *Consultant*, Eli Lilly; *Consultant*, Epizyme; Ivan Chebib: None; Vikram Deshpande: *Grant or Research Support*, Advanced Cell Diagnostics; *Advisory Board Member*, Viela; *Grant or Research Support*, Agios Pharmaceuticals

Background: *NTRK* gene fusions are detected in a wide variety of adult and pediatric tumors and are oncogenic drivers in tumor formation. *NTRK* is a clinically actionable genetic alteration regardless of tumor histology. DNA/RNA sequencing-based assays represent the gold standard for diagnosis, although, pan-TRK immunohistochemistry (IHC) may serve as a surrogate marker with a reported sensitivity and specificity of 95 and 100%, respectively. Additionally, pan-TRK IHC is used as a diagnostic tool in tumors with a high prevalence of *NTRK* rearrangement. Herein, we assess the efficacy of RNA in situ hybridization (ISH) platform as a surrogate marker for *NTRK* fusions.

Design: We initially evaluated two cohorts in this study. Cases in the first cohort included *NTRK* fusion-positive (n=8) and fusion-negative tumors (n=8) identified by fusion assay. Cases in the second cohort included *NTRK* associated mesenchymal tumors (n=9). RNA in situ hybridization (ISH) was performed using pan-NTRK probe (Hs-NTRK pool, RNAScope® 2.5 LS, Advanced Cell Diagnostics). We graded NTRK ISH positivity semi-quantitatively as grade 1, 2, and 3. Grading was performed as follows: Grade 1 for staining conspicuous at 400x magnification, Grade 2 at 100x magnification and Grade 3 at 20x magnification. We compared these results to reactivity with pan-TRK IHC (EPR17341, Abcam). Following these cohorts, we evaluated a third cohort which included synovial sarcoma cases (n=83). We performed pan-TRK IHC and pan-NTRK ISH in these cases.

Results: All eight *NTRK* fusion-positive cases in the first cohort, including *NTRK1*, *NTRK2*, and *NTRK3* fusions, were positive for pan-NTRK RNA ISH. All eight *NTRK* fusion-negative tumors in the first cohort were negative for pan-TRK IHC and ISH. All mesenchymal tumors including infantile fibrosarcoma (n=4) and lipofibromatosis-like neural tumor (n=4) were positive for both the pan-TRK IHC and ISH. In the third cohort, we identified two synovial sarcoma cases (2.4% of the cases) positive for both pan-NTRK ISH and pan-TRK IHC.

Case (Cohort #-Case#)	Diagnosis	Age	Gender	Site	NTRK- Fusion	pan-TRK IHC	pan-NTRK ISH
1-1	Papillary Thyroid Carcinoma	67	F	Thyroid Gland	RBPMS-NTRK3	Positive	3+
1-2	Papillary Thyroid Carcinoma	21	F	Thyroid Gland	RBPMS-NTRK3	Positive	2+
1-3	Mammary Analog Secretory Carcinoma	25	M	Parotid Gland	ETV6-NTRK3	Positive	2+
1-4	Metastatic Papillary Thyroid Carcinoma	78	M	Brain	EML4-NTRK3	Positive	2+
1-5	Low-Grade Glioneuronal Tumor	54	M	Brain	BCAN-NTRK1	Positive	3+
1-6	Papillary Thyroid Carcinoma	74	F	Thyroid Gland	ETV6-NTRK3	Positive	3+
1-7	Papillary Thyroid Carcinoma	24	M	Thyroid Gland	TPR-NTRK1	Positive	3+
1-8	Low-Grade Neuronal Tumor	26	M	Brain	SDCCAG8-NTRK2	Not performed	2+
2-1	Lipofibromatosis-Like Neural Tumor	17	M	Thigh	NA	Positive	2+
2-2	Infantile Fibrosarcoma	3m	M	Buttock	ETV6-NTRK3	Positive	3+
2-3	NTRK-Rearranged Spindle Cell Neoplasm (NOS)	26	M	Palm	NA	Positive	3+
2-4	Lipofibromatosis-Like Neural Tumor	8	M	Forearm	NA	Positive	2+
2-5	Infantile Fibrosarcoma	22d	F	Leg	ETV6-NTRK3	Positive	2+
2-6	Lipofibromatosis-Like Neural Tumor	6	M	Abdominal wall	NA	Positive	2+
2-7	Lipofibromatosis-Like Neural Tumor	10	M	Abdominal wall	NA	Positive	2+
2-8	Infantile Fibrosarcoma	3m	F	Vertex	ETV6-NTRK3	Positive	2+
2-9	Infantile Fibrosarcoma	7d	F	Paraspinal	ETV6-NTRK3	Positive	3+

Conclusions: Pan-NTRK ISH could serve as a surrogate marker of *NTRK* fusions and may have a role in cases in which IHC results are ambiguous. Combined use of pan-TRK ISH and IHC could also be used to screen for *NTRK* fusion positive neoplasms.

836 Melanomas Usually Express E-Cadherin and Occasionally Express EMA and Keratin AE1/AE3 Creating Potential Diagnostic Confusion with Carcinoma

Nicholas Caldwell[1], Ilham Farhat[1], Jon Thomason[1], Felipe Nör[2], Andrew Bellizzi[1], Sarag Boukhar[1]
[1]University of Iowa Hospitals and Clinics, Iowa City, IA, [2]University of Iowa College of Dentistry, Iowa City, IA

Disclosures: Nicholas Caldwell: None; Ilham Farhat: None; Jon Thomason: None; Felipe Nör: None; Andrew Bellizzi: None; Sarag Boukhar: None

Background: Broad-spectrum epithelial markers including cytokeratins, epithelial membrane antigen (EMA), and monoclonal antibodies to EpCAM (i.e., MOC-31, Ber-EP4) are frequently used in characterizing undifferentiated tumors, with positivity used to support a diagnosis of carcinoma. Melanoma is known to occasionally express at least some of these markers, which leads to significant diagnostic confusion and potentially delayed diagnosis. We sought to systematically evaluate broad-spectrum epithelial marker expression in a large cohort of melanomas.

Design: E-cadherin, EMA, AE1/AE3, MOC-31, Ber-EP4, and BRAF V600E immunohistochemistry (IHC) was performed on tissue microarrays (TMAs) of 276 melanomas from 251 patients (142 male, 109 female) with an average age of 68 (24 to 105). These included 137 primaries (90% skin, 5% sinonasal, 5% other) and 139 metastases (32% lymph node, 18% brain/dura, 14% bone/soft tissue, 36% other). Epithelial IHC was scored for intensity (0-3+) and extent (0-100%), and H-score (intensity*extent) was calculated; BRAF V600E IHC was scored as positive or negative. The relationship between broad-spectrum epithelial marker expression and clinicopathologic variables was examined using Fisher's exact and Mann Whitney tests ($p<0.05$ considered significant).

Results: Melanomas very frequently expressed E-cadherin (75%), followed by EMA (16%) and AE1/AE3 (9%); MOC-31 and Ber-EP4 were never positive. The median E-cadherin H-score in metastases (112) exceeded that in primaries (80) (p-value 0.009). No other comparison was significant. Detailed data are presented in the Result Table.

Association of Broad-Spectrum Epithelial Markers Positivity to Clinicopathologic Variables

	E-cadherin positive	EMA positive	AE1/AE3 positive									
	n (%)	p-value	H-score Mean (median)	p-value	n (%)	p-value	H-score Mean (median)	p-value	n (%)	p-value	H-score Mean (median)	p-value
Overall	207 (75)		109 (97) Range: 2-300		45 (16)		21 (10) Range: 2-107		24 (9)		54 (20) Range: 3-260	
Men	115 (75)	0.9	120 (106)	0.2	24 (16)	0.7	22 (12)	0.6	10 (7)	0.19	65 (48)	0.5
Women	92 (76)		97 (80)		21 (17)		19 (10)		14 (11)		47 (18)	
Primary	105 (77)	0.5	94 (80)	0.009	25 (18)	0.4	23 (17)	0.49	10 (7)	0.5	51 (23)	0.8
Metastasis	102 (74)		95 (112)		20 (14)		18 (7)		14 (10)		56 (20)	
BRAF Positive	65 (84)	0.04	99 (87)	0.17	12 (16)	1.0	20 (7)	0.8	10 (13)	0.1	60 (38)	0.7
BRAF Negative	142 (72)		114 (103)		33(17)		21 (13)		14 (7)		50 (18)	
Cutaneous	177 (76)	0.69	110 (97)	0.7	40 (17)	0.5	22 (13)	0.2	20 (9)	0.7	60 (23)	0.3
Non-cutaneous	30 (73)		106 (87)		5 (12)		8 (3)		4 (10)		23 (20)	

Conclusions: 1. E-cadherin positivity is frequently seen in primary and metastatic melanoma (with stronger expression in the latter) and should not be used as a broad-spectrum epithelial marker. 2. EMA and keratin AE1/AE3 are occasionally expressed, as such, do not exclude a diagnosis of melanoma. 3. MOC-31 and Ber-EP4 demonstrate the highest negative predictive value for melanoma in our cohort.

837 Detection of ALK Gene Rearrangements in Lung Adenocarcinomas: Assessment of Concordance Among IHC, FISH, RNA ISH, and NGS Testing Modalities

Carleigh Canterbury[1], Helen Fernandes[2], Murty Vundavalli[3], John Crapanzano[3], Matthias Szabolcs[3], Anjali Saqi[3]
[1]Columbia Medical Center, New York, NY, [2]Columbia University, New York, NY, [3]Columbia University Medical Center, New York, NY

Disclosures: Carleigh Canterbury: None; Helen Fernandes: None; Murty Vundavalli: None; John Crapanzano: None; Matthias Szabolcs: None; Anjali Saqi: None

Background: *ALK*-rearrangement is present in 3-5 % of lung carcinomas, and if present, patients may benefit from targeted tyrosine kinase inhibitors. The 2018 updated molecular testing guidelines for lung cancer patients incorporated ALK immunohistochemical (IHC) analysis as an equivalent to fluorescent *in situ* hybridization (FISH) analysis recommended in 2013. However, no specific recommendation for use of alternative methods were proposed due to the lack of sufficient data. The aim of this study was to compare results of ALK IHC, FISH, DNA and RNA NGS, RNA in situ hybridization (RNA ISH) and circulating tumor DNA (ctDNA).

Design: Testing was performed on 2 groups. Group 1: Cases with ALK IHC, break-apart ALK FISH, targeted DNA NGS, and targeted RNA NGS (Archer) were retrieved and positive/negative results for each were recorded. RNA ISH was performed on cases ALK positive by any

modality. Group 2: Cases negative by ALK IHC and FISH also underwent RNA ISH. A positive result using RNA ISH is defined as 2 signals per cell in at least 5% of cancer cells and at least 1 cancer cell with 4 or more signals. When available, results were correlated with ctDNA and outcomes of patients treated with targeted inhibitors.

Results: Group 1 comprised 57 unique patient cases. All available tests but one were concordant for ALK (16 and 40 positive and negative, respectively). The one discordant case was FISH positive, RNA ISH positive, and IHC negative; RNA NGS is pending. Group 2 comprised 25 cases all of which were negative by IHC, FISH, and RNA ISH (Table 1). The RNA NGS fusion assay allowed detection of novel and rare fusion partners SLMAP and TFG, respectively. ctDNA (Guardant) was available for 2 positive cases and showed identical rearrangements as detected by RNA NGS in both cases. The single patient with discordant results had disease progression on targeted therapy with alectinib.

Table 1. Clinical characteristics of ALK rearrangements

		Cases examined	Median age[a] (age range)	Male:Female	IHC	FISH	RNA NGS	RNA ISH	ctDNA
Group 1	**Concordant Positive**	16	63(29-90)	9:7	16/16 (100%)	16/16 (100%)	16/16 (100%)	14/14 (100%)[b]	2/2 (100%)
	Concordant Negative	40	70(53-88)	11:9	40/40 (100%)	40/40 (100%)	40/40 (100%)		
	Discordant	1	80	-	(-)	(+)	*	(+)	
Group 2	**Negative Controls**	25			25/25 (100%)	25/25 (100%)		25/25 (100%)	

*Results of this study are pending

[a]Age in years at the time of biopsy or resection

[b]Additional RNA ISH studies of concordant positive cases are pending

Conclusions: Our results demonstrate high level of concordance across the testing modalities. The one discordance was between ALK IHC and ALK FISH/RNA ISH results. RNA NGS can detect the specific ALK rearrangement, including novel ones, which may help identify patients who may or may not benefit from targeted therapy.

838 SOX10 is Frequently Strongly Expressed by Basaloid Squamous Cell Carcinoma across Anatomic Sites and only Rarely by Other Squamous Cell Carcinomas

Stephanie Chen[1], Anand Rajan KD[1], Andrew Bellizzi[1]
[1]*University of Iowa Hospitals and Clinics, Iowa City, IA*

Disclosures: Stephanie Chen: None; Anand Rajan KD: *Advisory Board Member*, Roche Diagnostics Corporation; Andrew Bellizzi: None

Background: SOX10 is a well-established melanocytic, nerve sheath, and myoepithelial differentiation marker. Last summer we encountered a "basaloid" anal squamous cell carcinoma (SCC) in which diffuse, strong SOX10-positivity raised the possibility of adenoid cystic carcinoma. Miettinen and colleagues (PMID: 25724000) had reported SOX10-positivity in 6% of 118 head and neck (HN) SCCs and 0% of 40 cutaneous ones, and we hypothesized an association with high-risk human papillomavirus (HPV). Rooper and colleagues (PMID: 30498968) subsequently reported SOX10-positiivty in 59% of 22 "true" basaloid HN SCCs vs 0% of 280 non-basaloid HN SCCs. Herein, we confirm and extend these findings.

Design: Initially, we performed SOX10 immunohistochemistry (IHC) on tissue microarrays (TMA) of 238 SCCs from diverse anatomic sites. Subsequently, we identified all in-house cases diagnosed as "basaloid SCC" (BSCC) or "SCC with basaloid features" from 1993-2015, and 3 reviewers independently reclassified them as BSCC, SCC with basaloid features, or neither based on WHO Head and Neck Blue Book criteria. SOX10 and p16 IHC were performed on a representative tissue block with SOX10-positivity scored as focal (F; ≤25% nuclei staining), multifocal (MF; 25-75%), or diffuse (D; >75%) and p16-positivity defined as ≥70% nuclear/cytoplasmic staining of at least moderate intensity. Tissue origins were coded as HN-HPV, HN-non-HPV, and other. Fisher's exact test was used with $p<0.05$ considered significant.

Results: SOX10-positivity was noted in 8% of 238 SCCs in TMA (17 F, 2 MF). Of 103 potential BSCCs, a diagnosis of definitive BSCC was made in 9, 11, and 20 cases by each of the 3 reviewers--with at least 2 reviewers agreeing in 12 and unanimous agreement in 7. SOX10-positivity was noted in 21 cases (12D, 7 MF, 2 F). MF to D SOX10-positivity was more frequent in cases called definitive BSCC by any observer (62% vs 7% in all other cases) and in those with consensus or unanimous agreement (83% vs 10% in all other cases)

(both p<0.0001) (Figure). The 12 (at least) consensus cases arose in the HN-HPV (5), HN-non-HPV (3), lung (2), and gynecological (GYN) tract (2); 5 were p16-positive (HN-HPV 4, GYN 1).

Figure 1 - 838

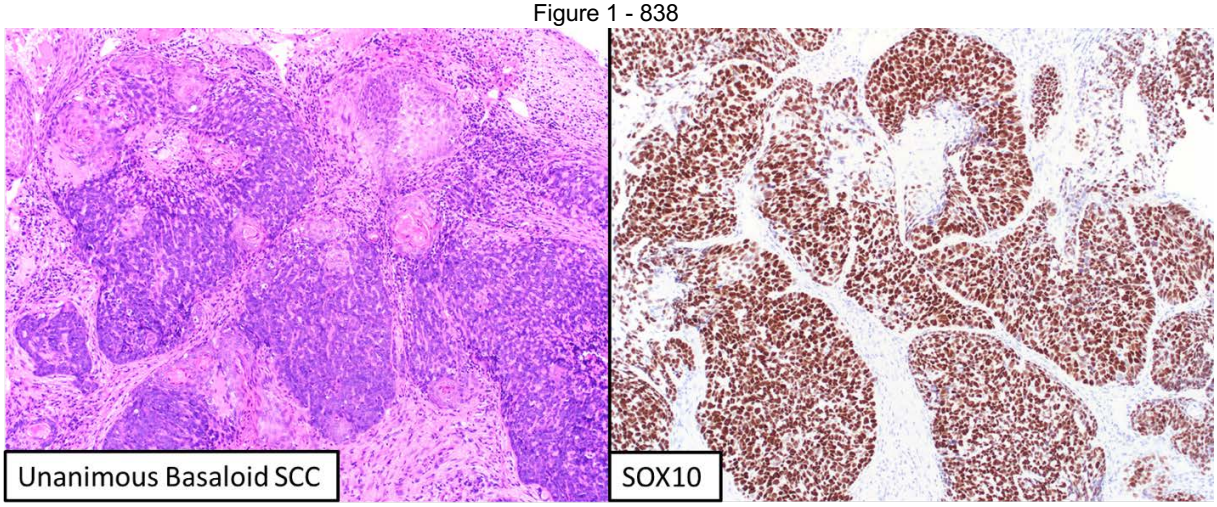

Conclusions: Strong SOX10-positivity is seen in most BSCCs and only rarely in other SCCs and should not dissuade from the diagnosis. "True" BSCC is uncommon, occurs at diverse anatomic sites, and may be p16-positive. SOX10-positivity in these cases likely reflects a component of myoepithelial differentiation.

839 BAP1 Inactivation is Rarely Observed by Immunohistochemistry in Cutaneous and Mucosal Melanoma

Ilham Farhat[1], Jon Thomason[1], Felipe Nör[2], Anthony Snow[3], Andrew Bellizzi[1], Sarag Boukhar[1]
[1]University of Iowa Hospitals and Clinics, Iowa City, IA, [2]University of Iowa College of Dentistry, Iowa City, IA, [3]North Liberty, IA

Disclosures: Ilham Farhat: None; Jon Thomason: None; Felipe Nör: None; Anthony Snow: None; Andrew Bellizzi: None; Sarag Boukhar: None

Background: *BAP1* (BRCA1-associated protein 1) is a tumor suppressor with roles in DNA repair, cell cycle regulation, differentiation, proliferation, and DNA damage responses. Germline mutations predispose to uveal melanoma, mesothelioma, renal cell carcinoma, and cutaneous melanoma. Somatic mutations are also frequently identified in uveal melanoma and mesothelioma and occasionally in renal cell carcinoma, with BAP1 inactivation identified in up to 80% of metastatic uveal melanomas. BAP1 immunohistochemistry (IHC) is an established surrogate marker for *BAP1*-mutation status. The goal of this study is to define the frequency of BAP1-inactivation, as assessed by IHC, in cutaneous and mucosal melanomas. If BAP1 loss is infrequent in these tumor types, BAP1 IHC could have a role in assessing metastatic melanomas of occult origin.

Design: BAP1 and BRAF V600E IHC was performed on tissue microarrays (TMAs) of 275 melanomas from 251 patients (142 male, 109 female) with an average age of 68 (24 to105). These included 137 primaries (90% skin, 5% sinonasal cavity, 5% other mucosal) and 138 metastases (32% to lymph nodes, 18% brain/dura, 14% bone/soft tissue, 36% other). BAP1 IHC was assessed as intact or lost; BRAF V600E mutation-specific IHC was assessed as positive or negative. Future plans include massively parallel sequencing of the entire coding region of *BAP1* to interrogate immunohistochemically positive samples for corresponding genetic lesions.

Results: BAP1 loss was seen in 9 of 275 cases (3%). Excluding 2 metastatic uveal melanomas, this represents 2% of 235 cutaneous, 17% of 6 sinonasal, 0% of 5 other mucosal, and 4% of unknown primary tumors. BAP1 inactivation was not significantly associated with BRAF V600E status (5 negative, 4 positive). Clinical annotation for the 9 BAP1-inactivated patients is presented in the Result Table.

Clinical Annotation of the BAP1-Inactivated Cases

	Age/ gender	Site	Primary (P) vs Metastasis (M)	Site of origin (subtype)	BRAF V600E IHC: Positive (P) vs Negative (N)	Follow up: Alive (A) or Deceased (D)	Other relevant findings
1	58/F	nasal cavity	P	Sinonasal	N	A	*BAP1* mutation identified in tumor tissue (c.422A>G:pH141R)
2	54/F	lymph node	M	Unknown primary	P	Unknown	*BRAF V600E* mutation confirmed by molecular; Unknown primary
3	34/F	lymph node	M	Cutaneous (Superficial Spreading)	P	Unknown	F/h of brain, lung, and ovarian tumors; melanoma in maternal uncle
4	68/M	skin, back	P	Cutaneous (nodular)	P	A	Unavailable
5	72/M	skin, buttock	P	Cutaneous (NOS)	N	Unknown	H/o cutaneous neurofibroma L upper chest
6	80/F	skin, foot	P	Cutaneous (nodular)	P	Unknown	H/o lentiginous compound nevus adjacent to prior resection
7	86/F	skin, thigh	P	Cutaneous (nodular)	N	D	Died of lung cancer metastatic to brain
8	44/F	liver	M	Uveal	N	D	Unavailable
9	73/F	stomach	M	Uveal	N	D	Unavailable

Conclusions: 1- BAP1 inactivation is rare occurrence in cutaneous and mucosal melanomas. 2- Loss of BAP1 expression in metastatic melanoma is highly suggestive of uveal origin. 3- There is no association between BAP1 and BRAF.

840 Life Cycle Assessment of Surgical Pathology Biopsies

Ilyssa Gordon[1], Jodi Sherman[2], Michael Leapman[3], Adam Nolte[4], Michael Overcash[5], Cassandra Thiel[6]
[1]Robert J. Tomsich Pathology & Laboratory Medicine Institute, Cleveland Clinic, Cleveland, OH, [2]Yale University, New Haven, CT, [3]Yale School of Medicine, New Haven, CT, [4]Mount Sinai Medical Center of Florida, Miami Beach, FL, [5]Wichita State University, Wichita, KS, [6]New York University School of Medicine, New York, NY

Disclosures: Ilyssa Gordon: None; Jodi Sherman: None; Michael Leapman: None; Adam Nolte: None; Michael Overcash: None; Cassandra Thiel: *Consultant*, Stryker

Background: The healthcare sector contributes 10% of US greenhouse gas emissions (GHGs). Given the adverse health effects associated with GHGs, healthcare sector workers have a moral imperative to reduce these GHGs. Life Cycle Assessment (LCA) is a tool used to quantify environmental emissions associated with a product or process, including natural resource extraction, manufacturing, packaging, transportation, use, and disposal of materials. To quantify GHGs and help guide pollution prevention strategies, we applied LCA to the process of preparing a biopsy in a surgical pathology laboratory.

Design: A detailed analysis of the processing of a biopsy was performed at a large surgical pathology laboratory, and grouped into 11 steps. Each supply item, reagent, and capital equipment was catalogued, along with the number of individuals involved, and average duration of each step. Supply items were weighed and primary material types noted. The lifespan of each reusable item was estimated, and post-use treatment pathways, including disposal, were noted. Reagent quantity was allocated to a single case based on total bottles used in the lab over one week. Watt meters and equipment power ratings were used to estimate the energy consumption of capital equipment. A lifecycle inventory and impact analysis were performed to estimate GHGs. The LCA was performed comparing two scenarios as a sensitivity analysis: (1) a patient case with a single biopsy jar and (2) a patient case with three biopsy jars.

Results: The largest proportion of total GHGs was from processing the cassette(s) on the tissue processor (Leica ASP 300S), which contributed 0.085kg of CO2-equivalents (kg CO2e) for scenario 1 and 0.224 kg CO2e for scenario 2, or, in both scenarios, 31% of total emissions, of which 25% was attributable to production of reagents used. The second largest contributor to GHGs was receiving and accessioning the case in the lab, which contributed 0.051kg CO2e or 19% of total emissions in scenario 1, and 0.151kg CO2e or 21% of total emissions in scenario 2, attributable mostly to the jars being single use items. Sensitivity analysis showed that GHGs can range between -18% and +4% for scenario 1, and between -15% and +10% for scenario 2.

Conclusions: This study evaluates the processing of a surgical pathology biopsy using an LCA. Understanding the process steps that contribute to GHGs is essential for determining which parts of the healthcare sector could be effectively targeted for reducing emissions.

841 Paraspinal Pseudoneoplasms: Varied Etiologies, Common Diagnostic Dilemmas. A Series of 66 Cases Emphasizing the Importance of Pathology-Radiology Correlation

John Gross[1], Stephen Broski[1], B. Howe[1], Andrew Folpe[1]
[1]Mayo Clinic, Rochester, MN

Disclosures: John Gross: None; Stephen Broski: None; B. Howe: None; Andrew Folpe: None

Background: A variety of non-neoplastic diseases of the spine, including herniated/sequestered intervertebral discs, synovial cysts, and degenerative or post-traumatic changes, may present as mass lesions. Over the past several years we have seen a large number of such paraspinal pseudoneoplasms in consultation, referred out of concern for malignancy on the part of the clinician, pathologist or both. Herein we review our experience with these specimens, emphasizing the clinical, radiographic and histopathological features that allow their confident distinction from various mesenchymal tumors.

Design: Cases from the paraspinal region, referred in consultation to exclude malignancy and diagnosed as showing non-neoplastic disease involving disc, spinal ligament or paraspinal soft tissues (n=66) were retrieved from our archives (2006-2019). Available radiographic studies were reviewed by one or more musculoskeletal radiologists. The histologic features of all cases were re-evaluated. Available clinical records were reviewed.

Results: Cases occurred in 37M and 29F (age range 26 to 88 years; mean 62 years) and involved the lumbar spine (n=24, 36%), thoracic spine (n=16, 24%), paraspinal/psoas/epidural/extradural regions (n=13, 19%), cervical spine (n=7, 10%), unknown spinal location (n=5, 7%), and sacral spine (n=1, 1%). Features concerning for a neoplastic process included: 1) degenerative/ reactive changes in disc/ spinal ligament, including bi-nucleation and mitotic activity (suggesting chondrosarcoma), 2) florid reactive vascular proliferation (misconstrued as angiosarcoma), 3) exuberant myofibroblastic and osteoclastic reaction (mimicking a spindle cell or osteoclast-rich neoplasm) and 4) reactive new bone formation (worrisome for an osteogenic tumor). Radiographic studies showed changes characteristic of various non-neoplastic processes, without evidence of a neoplasm.

Conclusions: Paraspinal pseudoneoplasms have various etiologies, including herniated/sequestered intervertebral disc, synovial cyst, trauma, and degenerative arthritis. Microscopic findings include degenerating disc and spinal ligament showing reactive nuclear changes, woven bone production, florid capillary proliferation growing in and around disc material, and peripheral myofibroblastic and osteoclastic proliferation. Awareness of this constellation of findings and radiographic correlation with experienced orthopedic radiologists should allow for confident diagnosis in almost all instances.

842 Lynch Syndrome: Immunohistochemical Patterns, Tumour Site, and Genetic Features

Elan Hahn[1], Melyssa Aronson[2], Thomas Ward[3], Kara Semotiuk[3], Spring Holter[4], Raymond Kim[5], Aaron Pollett[3]
[1]University of Toronto, Toronto, ON, [2]Zane Cohen Centre, Sinai Health System, Toronto, ON, [3]Mount Sinai Hospital, Toronto, ON, [4]Zane Cohen Centre for Digestive Diseases, Familial Gastrointestinal Cancer Registry (FGICR), Mount Sinai Hospital, Toronto, ON, [5]University Health Network, Toronto, ON

Disclosures: Elan Hahn: None; Melyssa Aronson: None; Thomas Ward: None; Kara Semotiuk: None; Spring Holter: None; Raymond Kim: None; Aaron Pollett: None

Background: Lynch syndrome (LS) is an autosomal dominant cancer predisposition syndrome caused by mutations in the mismatch repair (MMR) genes (*MLH1, MSH2, MSH6, PMS2, and EPCAM*). The tumours in patients with Lynch Syndrome typically show abnormal gene expression by immunohistochemistry (IHC). The objective of this study is to examine the relationship between the genetic mutation, tumour site, IHC staining, and clinical presentation.

Design: A retrospective analysis of tumours from 630 patients with proven LS were identified from an institutional registry. Tumour site, histology, IHC staining and Lynch syndrome genetic testing data, were extracted.

Results: 1019 tumours sampled were identified in the 630 patients. The average age of first presentation ranged from 40 (*PMS2* carriers) to 50 (*MSH6* carriers). Abnormal IHC staining was seen in 85% of tumours. Abnormal IHC staining varied widely between tumour sites ranging from 34% (breast) to 95% (stomach and esophagus). Abnormal IHC staining corresponded to the specific mutated gene in 79% of cases, ranging from 70% (*MSH6* carriers) to 85% (*MSH2* carriers); in other cases, the IHC findings did not correspond with the underlying germline mutation. Tumour site also varied with the underlying genetic mutation, with tumours from upper GI or urinary tract being more commonly associated with *MSH2* and brain tumours associated with *PMS2*.

Conclusions: Abnormal IHC expression can be seen in a wide range of tumours in patients with known LS, including a number of tumours not typically associated with LS. Not all LS-associated tumours in patients with known LS show abnormal mismatch IHC expression. Abnormal IHC staining does not always correspond to the underlying gene mutation, with some tumours showing intact staining for the known mutated gene, but deficient staining in other MMR genes. There is an association between specific gene mutations and clinical features, such as age at first presentation and tumour site. The variation of IHC staining in tumours of patients with LS, as well as the genotype-phenotype correlation, need to be recognized to ensure that patients with LS are appropriately identified and investigated.

843 SMAD4-Inactivation is Rare in Gastroesophageal Adenocarcinomas and does not Occur at Increased Frequency in Metastases

Robert Humble[1], Matthew Gosse[2], Ibrahim Abukhiran[1], Andrew Bellizzi[1]
[1]University of Iowa Hospitals and Clinics, Iowa City, IA, [2]Iowa City, IA

Disclosures: Robert Humble: None; Matthew Gosse: None; Ibrahim Abukhiran: None; Andrew Bellizzi: None

Background: For the last decade we have routinely used loss of SMAD4 expression to suggest a pancreatic origin in carcinomas of unknown primary, in particular in "CK7+ only" and CK20 and/or CDX2 weakly positive tumors. Although up to 30% of colon cancers are SMAD4-inactivated, these are uncommonly phenotypic mimics of pancreas cancer. We have done this somewhat cautiously, given a paucity of data on SMAD4 in upper gastrointestinal tract adenocarcinomas. A recent pan-carcinoma study seems to validate our approach, with Ritterhouse and colleagues reporting SMAD4 loss in 4% of 53 esophageal and 2% of 45 gastric cancers (PMID: 31054158). A single large study has given us pause, with Singhi and colleagues finding loss in 10% of 205 primary and 44% of 43 metastatic esophageal adenocarcinomas (PMID: 25634752).

Design: We assembled our institutional cohort (1991-2018) of gastroesophageal adenocarcinomas from which there was sufficient material to construct tissue microarrays. All original glass slides/pathology reports were reviewed for tumor epicenter (esophagus, GEJ, stomach), Lauren classification, tumor infiltrating lymphocytes (TIL), and pTNM; age and gender were recorded; SMAD4 (clone EP618Y) and MMR immunohistochemistry was performed. Chi-square tests were used with $p<0.05$ considered significant.

Results: We examined 339 samples (229 primaries, 81 lymph node metastases, 25 distant metastases, and 4 clinical recurrences) from 249 patients (206M:43W; 64% intestinal, 15% diffuse, 12% mixed, 9% other; 14% with conspicuous TILs; 2.4% MMR-deficient). These included 109 esophageal, 68 gastroesophageal junction (GEJ), and 72 gastric cancers. SMAD4 inactivation was seen in 24 samples from 19 patients, representing 10% of esophageal, 7% of GEJ, and 4% of gastric cancers ($p=0.3$). They had no special clinicopathologic features relative to the entire cohort (16M:3W; 14 intestinal, 5 mixed; 21% with conspicuous TILs; 4 pT1b, 1 pT2, 11 pT3, 2 pT4; all MMR-proficient). Overall, 6% of primaries, 11% of lymph node metastases, 4% of distant metastases, and 0% of clinical recurrences demonstrated absent SMAD4 staining ($p=0.4$ for primaries vs all others).

Conclusions: SMAD4 inactivation was relatively uncommon in our cohort and occurred at a similar frequency in primaries and advanced disease. This would seem to validate our use of loss of SMAD4 expression to suggest a pancreatic origin in "CK7 only" and CK20 and/or CDX2 weakly positive metastases of occult origin.

844 Merkel Cell Carcinoma of Lymph Node is Metastatic Cutaneous Merkel Cell Carcinoma

Lauren Lawrence[1], Christian Kunder[2], Henning Stehr[1], Atif Saleem[3], Yaso Natkunam[4], James Zehnder[2], Benjamin Pinsky[5], Malaya Sahoo[6], Susanna Tan[6]
[1]Stanford University, Stanford, CA, [2]Stanford University School of Medicine, Stanford, CA, [3]Stanford University, San Jose, CA, [4]Stanford University Medical Center, Stanford, CA, [5]Stanford, Palo Alto, CA, [6]Stanford, Stanford, CA

Disclosures: Lauren Lawrence: None; Christian Kunder: None; Henning Stehr: None; Atif Saleem: None; Yaso Natkunam: None; James Zehnder: None; Benjamin Pinsky: None

Background: The differential diagnosis for a metastatic neuroendocrine carcinoma of unknown primary includes metastatic Merkel cell carcinoma and metastases from other primary sites with described neuroendocrine carcinomas, including the lung and gastrointestinal tract. The possibility of a so-called “primary lymph node neuroendocrine carcinoma” has been described in the literature, relying on such characteristics as absence of a known primary and features such as weak immunohistochemical expression of PAX5 and TdT in some cases. Here we evaluate cases of neuroendocrine carcinoma of unknown primary at our institution.

Design: Samples evaluated for this study include 6 cases of ‘primary lymph node Merkel cell carcinoma’ and 1 case of metastatic neuroendocrine carcinoma at a bony site, all with unknown primary. Exome and targeted panel sequencing generated somatic variants for use in mutational signature analysis as well as use of off-target reads with alignment to the Merkel cell polyoma virus (MCPyV) genome. Real-time PCR was also employed as an orthogonal method for the detection of MCPyV.

Results: The cases show a preponderance of immunohistochemical positivity for CK20, with molecular evidence by of either ultraviolet (UV) mutational signature or off-target alignment of Merkel cell polyomavirus in all evaluated cases. Four of six 'primary lymph node' cases were positive for a UV mutational signature, with the remaining two cases were positive for off-target alignment and RT-PCR of MCPyV. One case of neuroendocrine carcinoma at a bony site was also positive for a UV mutational signature and showed RT-PCR positive for MCPyV below the limit of quantitation (with no off-target reads of MCPyV).

Case/Control Status	Off-target Alignment of Merkel Cell Polyoma Virus	UV Mutational Signature	Sequencing	Paired Normal Tissue Sequenced?	Site	CK20	Variants Analyzed	Summed Error
Case	Positive	Negative	Exome	Yes	Axillary lymph node	Perinuclear dot-like	119	0.079
Case	Negative	Positive	Exome	No	Submandibular lymph node	Dot-like	682	0.05
Case	Negative	Positive	Exome and Targeted Panel	Yes	Level II lymph node	"Diffusely positive"	1589 (exome); 11 (targeted panel)	0.058 (exome); 0.238 (targeted panel)
Case	Negative	Positive	Exome	No	Scapula/bony site	Perinuclear dot-like	1737	0.061
Control	Negative	Negative	Exome	Yes	Parotid gland lymph node	Not performed	574	0.052
Control	Negative	Negative	Exome	No	Neck lymph node	Not performed	379	0.061
Case	Negative	Positive	Targeted Panel	No	Cervical lymph node	Perinuclear dot-like	10	0.266
Case	Negative	Positive	Targeted Panel	No	Submandibular soft tissue (?lymph node?)	Membranous and focal perinuclear dot-like	13	0.233
Case	Positive	Excesseive summed error; negative	Targeted Panel	No	Inguinal lymph node	Perinuclear dot-like	2	0.932

Figure 1 - 844

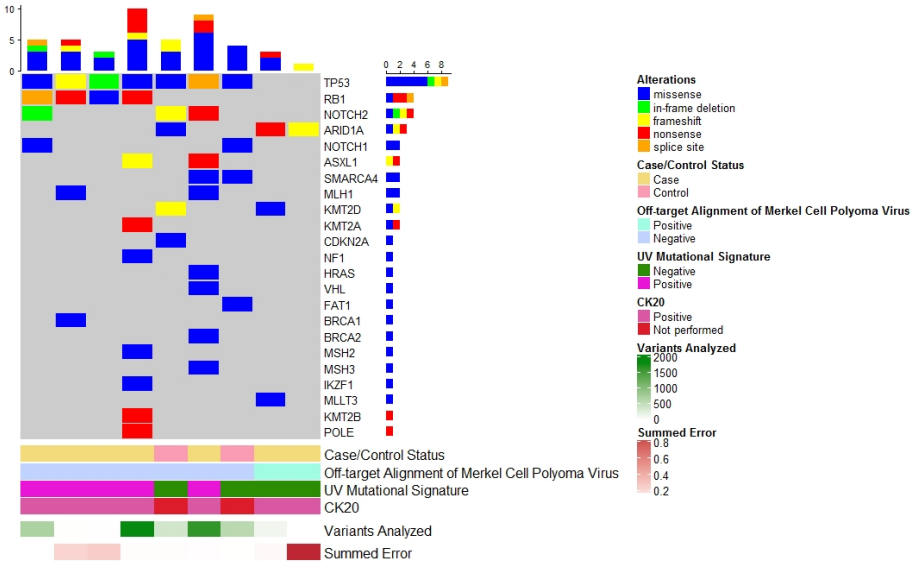

Figure 2 - 844

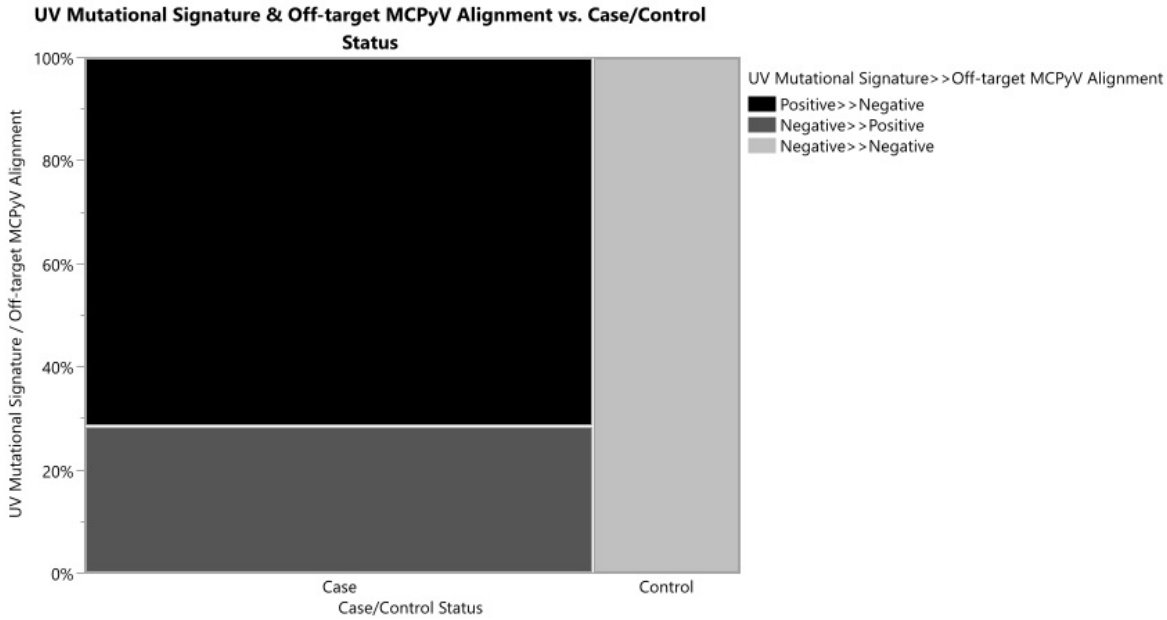

Conclusions: Given that UV radiation and MCPvV are not understood to represent etiologic factors in lymphoma, we conclude that neuroendocrine carcinoma of unknown primary with characteristics consistent with Merkel cell carcinoma is unlikely to represent a process primary to the lymph node, and that cases documented at our institution are metastases from regressed (or mis-diagnosed) cutaneous primaries. In sum, in the small number of cases of metastatic neuroendocrine carcinoma of unknown primary, characteristics consistent with Merkel cell carcinoma, and sufficient tissue for analysis at our institution, all have findings consistent with metastatic Merkel cell carcinoma originating at a cutaneous site. We find no evidence to corroborate the existence of so-called primary lymph node Merkel cell carcinoma.

845 Comparison of the Performance of Two Different ALK Antibody Clones (D5F3 and ALK1) in Anaplastic Large Cell Lymphoma (ALCL)

Dana Martin[1], Steven Smith[2], Terra Lewis[1], Raghavendra Pillappa[3]
[1]Virginia Commonwealth University Health System, Richmond, VA, [2]Virginia Commonwealth University School of Medicine, Richmond, VA, [3]Virginia Commonwealth University Health System, Glen Allen, VA

Disclosures: Dana Martin: None; Steven Smith: *Consultant*, Elsevier Publishing/Amirsys; Terra Lewis: None; Raghavendra Pillappa: None

Background: Anaplastic large cell lymphoma (ALCL) is a T-cell lymphoma characterized by CD30 expression and subdivided into anaplastic lymphoma kinase (ALK) positive and negative subtypes that may show clinically significant differences in outcomes. The current standard for evaluating ALK status is immunohistochemistry using the mouse monoclonal anti-human CD246 (ALK1) or fluorescence in situ hybridization. The novel rabbit monoclonal anti-human CD246 (D5F3) is proposed as an alternative to ALK1 and FDA approved for diagnosis of ALK-rearranged lung adenocarcinoma. However, its performance has not been systematically tested and compared to ALK1 in ALCL.

Design: Nineteen cases of ALCL were identified from institutional database searches and retrieved. A representative slide from each case was stained using ALK1 and D5F3 in an automated slide stainer. The intensity of cytoplasmic staining (graded 0-3, none, faint, moderate and strong) and percentage of positive cells (0, <5, 5-50%, 50-75% and >75%) were evaluated for each individual clone and subsequently compared between the two clones.

Results: Of the nineteen cases, five were previously diagnosed as ALK expression positive by ALK-1 staining. Five cases were positive for ALK expression by ALK1 staining (26.3%; 1 1+; 0 2+; 4 3+), while nine were positive by D5F3 staining (47%; 3 1+. 1 2+; 5 3+). There were no cases that were positive by ALK1, but not by D5F3, which had identified the five additional cases. For three of the five cases (60%) positive by both stains, the D5F3 stained slides showed greater percentage of cells stained. The staining intensity was greater by D5F3 in one of five cases, the other four cases showed the same (3+) intensity by D5F3 and ALK1. FISH results are available in three cases (15.7%) and demonstrated 100% concordance with ALK expression by both IHC stains (two positive, one negative).

Conclusions: These findings support the use of D5F3 as an equivalent and potentially more sensitive alternative to ALK1 for the evaluation of ALK positivity in ALCL.

846 An Immunohistochemical Comparison of H3K27me2 and H3K27me3 Expression with Emphasis on Malignant Peripheral Nerve Sheath Tumors (MPNST), Diffuse Midline Glioma and Melanoma

Brooke McCann[1], Anja Roden[1], Caterina Giannini[1], Andrew Folpe[1]
[1]Mayo Clinic, Rochester, MN

Disclosures: Brooke McCann: None; Anja Roden: None; Caterina Giannini: None; Andrew Folpe: None

Background: A subset of MPNST shows loss of function mutations affecting *EED* or *SUZ12* genes, which encode the core subunit of the polycomb repressive complex 2 (PRC2). Loss of PRC2 activity results in loss of trimethylated histone H3 at lysine 27 (H3K27me3). Complete loss of H3K27me3 expression is present in roughly 60% of NF1-associated and >90% of sporadic or post-irradiation MPNST, with retained expression seen in neurofibromas and epithelioid MPNST. However, H3k27me3 loss of expression is also seen in significant subsets of synovial sarcoma (SS), dermatofibrosarcoma (DFSP) and melanoma, limiting the diagnostic utility of this marker. A very recent study has suggested that histone H3 dimethyl (H3k27me2) loss is highly specific for MPNST, distinguishing true PRC2 loss from isolated H3k27me3 loss. We compared the expression of H3k27me3 and H3k27me2 in a large series of well-characterized MPNST and related lesions.

Design: FFPE sections from 26 MPNST, 11 neurofibromas (NF), 9 DFSP, 9 SS, 13 diffuse midline glioma H3K27M-mutant (DMG), 2 conventional diffuse astrocytoma, 8 cutaneous melanoma (CM) and 8 ocular melanoma (OM) were immunostained for H3k27me2 (Abcam, rabbit polyclonal, 1/1500) and H3k27me3 (Cell Signaling, clone C36B11, 1/50), using the Ventana Benchmark Ultra autostainer, Ultra CC1 pretreatment, antibody incubation at 36°C, Optiview DAB detection and Hematoxylin II counterstaining.

Results: The immunohistochemical results are summarized in the Table. Overall, H3k27me3 and H3k27me2 results were concordant in 69 of 86 (80%) cases. Loss of H3k27me3 with retained H3k27me2 was seen in 10 cases (12%); loss of H3k27me2 with retained H3k27me3 occurred in 7 cases (8%). Loss of H3k27me2 alone was seen only in melanoma, 6 of 7 (86%) of which were OM. This pattern was seen in 6 of 8 (75%) OM and only 1 of 8 (13%) CM.

Tumor Type	H3k27me3 retained & H3k27me2 retained	H3k27me3 lost & H3k27me2 lost	H3k27me3 lost & H3k27me2 retained	H3k27me3 retained & H3k27me2 lost
MPNST (n=26)	8	14	4	0
NF (n=11)	11	0	0	0
DFSP (n=9)	9	0	0	0
SS (n=9)	9	0	0	0
DMG (n=13)	0	9	4	0
Astrocytoma (n=2)	1	0	1	0
CM (n=8)	4	2	1	1
OM (n=8)	0	2	0	6

Conclusions: In agreement with a prior study, we have found generally good concordance between H3k27me3 and H3k27me2 staining. Loss of H3k27me3 with retained H3k27me2, seen most often in MPNST and MG, likely reflects isolated H3k27me3 loss in the absence of PRC2 loss, and should be interpreted with caution in the diagnosis of these tumor types. Interestingly, loss of H3k27me2 with retained expression of H3k27me3 seems to be a feature only of melanoma, in particular OM. Further investigation is needed to determine whether this is related to the different molecular pathogenesis of OM as compared with CM.

847 Clinicopathological Features of IgG4-Related Disease: An Institutional Experience

Pritinanda Mishra[1], Susama Patra[1], Mukund Sable[1], Suchitra Kumari[1]
[1]All India Institute of Medical Sciences, Bhubaneswar, Odisha, India

Disclosures: Pritinanda Mishra: None; Mukund Sable: None

Background: IgG4 - related disease (IgG4-RD) is a newly described entity showing multisystem involvement with typical inflammatory lesions resembling pseudotumors. This entity is rich in IgG4 positive plasma cells, fibroblastic proliferation and often but not always elevated serum IgG4 concentrations. Inflammatory lesions without any specific cause are being diagnosed as IgG4-RD.

Design: This is retrospective and prospective study (January 2017 to January 2018) of all cases showing mass lesions with histopathological suspicion of chronic inflammation or inflammatory pseudotumors. Cases diagnosed as lymphoma, autoimmune disorder and Castleman diseases were excluded. Serum IgG &IgG4 was done based on two-site sandwich enzyme immunoassay principle.

Relevant clinical details like age, gender, site specific involvement, radiological findings were documented. Histological findings ie. composition of the inflammatory infiltrate, irregular /storiform fibrosis, and obliterative phlebitis with semi-quantification of the lymphoplasmacytic infiltrate were noted. Immunohistochemical staining for IgG4 was performed. All cases were graded as pattern A, B and C based on percentage of inflammatory cells and fibrosis.

Results: Fifteen out of 94 biopsies from mass lesions (15.9%) were diagnosed as IgG4-RD. All the fifteen patients were adults except one and the mean age of presentation was 38.9 years (range 14 - 64 years). There was female preponderance (M:F=1:4). None of our patients had multiorgan involvement. The sites of involvement were orbit (n=4), breast (n=2), lung (n=2), nasal sinus (n=2), ear mass (n=2), cervical nodes (n=1), paraspinal mass (n=1) and submandibular gland (n=1). Clinical features are summarized in table 1. Serum IgG4 was elevated in 11/13 patients, while normal in 2/13 cases. Histology showed storiform fibrosis (100%), obliterative phlebitis (28.5%) and sheets of plasma cells (100%) admixed with lymphocytes (100%), eosinophils (100%), macrophages (71.4%) and neutrophils (0%). Pattern A was seen in 8/14 cases, pattern B in 5/14 and pattern C 1/14 cases. Lymphoid follicle formation was noted in two cases (14.2%). Eight patients after a period of 10 months of treatment did not show any recurrence.

Case no	Age (yrs)	Gender	Organ involved	Clinical presentation	Radiological features	Clinical diagnosis	HPE diagnosis	Serum IgG4 levels(mg/dl)	Treatment
Case 1	55	F	Breast (R)	Retroareolar lump	BIRADS III	Mastitis	IgG4-RD	NA	Steroids
Case 2	52	F	Breast (L)	Upper outer quadrant	BIRADS II	Carcinoma	IgG4-RD	40	Steroids
Case 3	40	F	Lacrimal glands (B/L)	Peri orbital swelling	CT-symmetric enlargement of lacrimal glands	? Carcinoma ?Pseudotumor	IgG4-RD	186	Steroids
Case 4	14	F	Para nasal sinus	Headache with diminished vision	Left sphenoid mass with parasellar extension	?Neurogenic tumor ?Lymphoma ?LCH	IgG4-RD	58	Steroids
Case 5	48	M	Para nasal sinus	Difficulty in nasal breathing and stuffiness	Soft tissue density in various PNS	Rhinoscleroma	IgG4-RD	432	Steroids
Case 6	35	M	Ear		Mass lesion	? Carcinoma	IgG4-RD	246	Steroids
Case 7	23	F	Ear		Mass lesion	?Carcinoma	IgG4-RD	160	Steroids
Case 8	28	F	Lung	Cough	Well defined heterogenous mass in RUL	?Bronchial adenoma	IgG4-RD	262	Steroids
Case 9	50	M	Lung	Cough	Heterogenous mass in RUL	? Bronchogenic carcinoma	IgG4-RD	249	Steroids
Case 10	21	F	Lymph node	Swelling	Multiple b/l cervical lymphadenopathy	? Tuberculosis	IgG4-RD	570	Steroids& rituximab
Case 11	19	F	Lacrimal glands(b/l)	Periorbital swelling	CT-symmetric enlargement of lacrimal glands	?lymphoma	NA	204	Steroids
Case 12	64	F	Orbit			?invasive aspergillosis	IgG4-RD	140	Orbital exenteration
Case 13	52	F	Submandibular gland	Painless mass	Diffuse enlargement of the gland	? PA	IgG4-RD	220	Excision and steroids
Case 14	45	F	Paraspinal mass			?	IgG4-RD	NA	Excision
Case 15	38	F	Orbital mass	Proptosis	Ill defined hyperechoic mass	? lymphoma	IgG4-RD	180	Excision and steroids

Figure 1 - 847

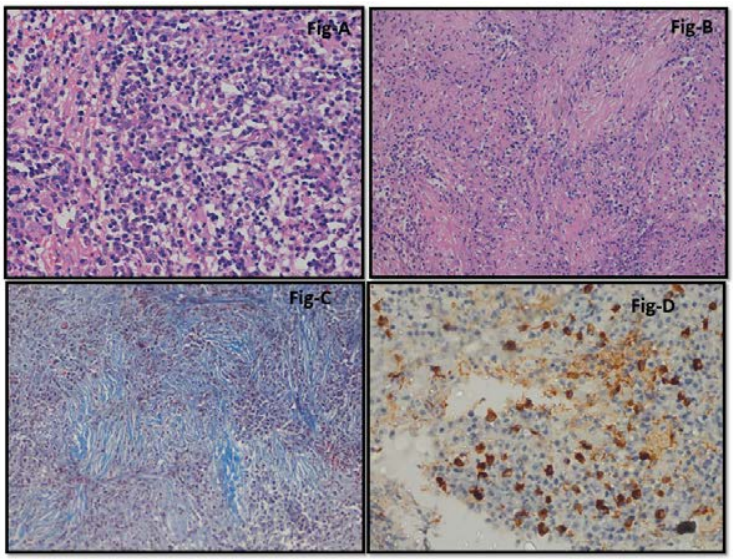

Conclusions: This rare benign entity, can masquerade as neoplastic lesions both in clinical setting and imaging studies. It is imperative to diagnose this entity correctly, as it requires medical management. The clue for diagnosis is a careful histopathological examination with ancillary adjuncts.

848 Gastrointestinal Tract (GIT) Lymphomas: Five-Year Institutional Experience at a University Teaching Center

Mitul Modi[1], Rifat Mannan[2]
[1]Pennsylvania Hospital of University of Pennsylvania Health System, Philadelphia, PA, [2]Perelman School of Medicine at the University of Pennsylvania, Philadelphia, PA

Disclosures: Mitul Modi: None; Rifat Mannan: None

Background: GIT is known to harbor various hematolymphoid neoplasms. Though relatively uncommon among all GIT cancers, primary GIT lymphomas account for 30%-40% of all extranodal lymphomas. These can be heterogeneous, involving various parts of luminal GIT. We sought to analyze the spectrum of GIT lymphomas diagnosed at our institute.

Design: We identified 47 cases of GIT lymphomas (2014-2018). Electronic medical records were reviewed for clinical details. Histology was reviewed for type of lymphoma, site of involvement and IHC/molecular findings as available.

Results: Detailed results are presented in table 1. Mean age was 67 years (range 29 -85); 34 male & 13 female. Different primary GIT lymphomas were: diffuse large B cell lymphoma (DLBCL, 40%, 19/47), marginal zone lymphoma (MZL, 34%, 16/47), follicular lymphoma (FL: 9%, 4/47), mantle cell lymphoma (4%, 2/47), Chronic Lymphocytic Leukemia/Small Lymphocytic Lymphoma (4%, 2/47), post-transplant lymphoproliferative disorders (4%, 2/47), classical Hodgkin lymphoma(CHL:2%, 1/47) & peripheral T cell lymphoma (2%, 1/47). Stomach (n=19, 40%) was the most common primary site for all GIT lymphomas, followed by small intestine (SI) (n=18, 38%), while esophagus was the least common (n=1, 2%). DLBCLs were most commonly located in stomach (n=10) followed by SI (n=7). MZLs were also most commonly found in stomach (n=10), followed by SI (n=2). All cases of FL originated in SI (n=4). Molecular studies were used to support diagnosis when required.

Table1: Characteristics of different GIT lymphomas

Type of Lymphoma	Males	Females
1. Diffuse Large B Cell Lymphoma	15	4
2. Marginal zone lymphoma	9	7
3. Follicular Lymphoma	4	0
4. Mantle Cell Lymphoma	1	1
5. Small Lymphocytic lymphoma (SLL/CLL)	1	1
6. Post-transplant lymphoproliferative disorder (PTLD)	2	0
7. Classical Hodgkin Lymphoma	1	0
8. T Cell Lymphoma	1	0

Common Sites of All GI Lymphomas Combined	
Site	**Number of Cases**
Stomach	19
Small Intestine	18
Colon	9
Esophagus	1
TOTAL	47

Conclusions: Our data suggests that DLBCL is the most common lymphoma involving GIT. Stomach is the most common location where both DLBCL and MZL can occur. Follicular lymphomas have a propensity for involving SI. These findings corroborate with previous studies of primary GIT lymphomas that, GIT lymphoma are mostly of B-cell lineage and distribution of histologic types was compatible with that of nodal lymphomas.

849 Precision and Repeatability of the VENTANA PD-L1 (SP263) Assay Across Six Different Tumor Types

Alma Nielsen[1], Guadalupe Manriquez[2], Dorothy Hayden[3], Fangru Lian[1], Chunyan Liu[1], Pallavi Patil[1], Peiyi Wang[1], Pengfei Gu[1], Karina Schnittker[1], Bryan Roland[1], Michelle Quiroz[1], Amy Hanlon Newell[4]
[1]Roche Tissue Diagnostics, Tucson, AZ, [2]Roche Tissue Diagnostics, Indianapolis, IN, [3]Roche Diagnostics, Tucson, AZ, [4]Ventana/Roche, Oro Valley, AZ

Disclosures: Alma Nielsen: None; Guadalupe Manriquez: None; Dorothy Hayden: *Employee*, Roche Molecular Solutions; Chunyan Liu: None; Pallavi Patil: *Employee*, Roche Tissue Diagnostic; Pengfei Gu: *Employee*, Roche; Bryan Roland: *Employee*, Roche; *Employee*, Roche; Amy Hanlon Newell: *Employee*, Roche; *Employee*, Roche

Background: PD-L1 IHC is the key biomarker and methodology to determine the eligibility of patients to immunotherapies in at least eight cancer types. Hence reliability and reproducibility of a PD-L1 assay across various tissue types is crucial. VENTANA PD-L1 (SP263) Assay has been approved in Europe for three PD-1/PD-L1 inhibitors in NSCLC and urothelial cancer (UC). Here we examine PD-L1 (SP263) precision and repeatability across 6 different disease indications: UC, NSCLC, Squamous Cell Carcinoma Head & Neck (SCCHN), Melanoma, Renal Cell Carcinoma (RCC), and Gastric Carcinoma. Data shows high level of consistency of PD-L1 (SP263) performance across these various tissue types.

Design: Formalin-fixed, paraffin-embedded (FFPE) specimens of each of the six different tissue types were assessed for precision and repeatability across readers, days, platforms, lots and labs by staining with the VENTANA PD-L1 (SP263) Assay (Fig.1). NSCLC, melanoma, RCC and gastric were evaluated by pathologists for percentage tumor cell staining (%TC) whereas UC and SCCHN were evaluated for both %TC and percentage immune cell staining (%IC). The samples were stratified as either positive or negative according to designated cut-offs. For each case, the modal result was determined and the result from each test sample was compared to its respective case-level modal result and deemed concordant or discordant. Results were aggregated across cases and the overall percent agreement (OPA) was calculated for each study (Table 1).

Results: All studies (Tab.1, Fig.1) showed high OPA for PD-L1 concordance to the designated cut-offs.

Figure 1. Intra-Day Repeatability [A] Squamous Cell Carcinoma of the Head and Neck (SCCHN) [B] Renal Cell Carcinoma (RCC) [C] Urothelial Carcinoma (UC) [D] Gastric or Gastroesophageal Junction (GEJ) Adenocarcinoma [E] Non-Small Cell Lung Carcinoma (NSCLC) [F] Melanoma

	Table1: Consistency and Repeatability of VENTANA PD-L1 (SP263) Assay in six indications						
Study	OPA						
	Inter-reader	Intra-reader	Inter-day	Intra-day	Inter-platform (GX, XT and ULTRA)	Inter-lot	Inter-lab
UC	93.0%	92.4%	100.0%	98.5%	98.8%	99.0%	92.6%
NSCLC	93.5%	96.2%	100.0%	100.0%	100%	100.0%	88.3%
SCCHN	98.0%	98.7%	90.0%	90.0%	99.2%	99.2%	98.6%
Melanoma	96.0%	96.0%	100%	100%	98.4%	98.4%	NA
RCC	100.0%	99.0%	100%	100%	100.0%	100.0%	93.2%
Gastric	99.3%	99.0%	100%	100%	100.0%	100.0%	NA

Conclusions: The data from the extensive precision studies shows that the VENTANA PD-L1 (SP263) Assay detects PD-L1 with high consistency and repeatability across a wide variety of disease indications. Further studies are ongoing these disease states to assess clinical utility.

850 Relatively Frequent "Aberrant" Expression of PAX8 by Mesothelial Proliferations: A Diagnostic Pitfall

Mohammad Obeidat[1], Andrew Bellizzi[1]
[1]*University of Iowa Hospitals and Clinics, Iowa City, IA*

Disclosures: Mohammad Obeidat: None; Andrew Bellizzi: None

Background: PAX8 is the "best" pan-Müllerian and renal cell carcinoma marker and is at least as useful as TTF-1 for thyroid. Broad PAX8 immunohistochemical surveys from a decade ago demonstrated a lack of expression by pleural and infrequent expression by peritoneal mesothelioma. A few recent studies have highlighted not infrequent PAX8-positivity in peritoneal mesothelial proliferations--a diagnostic pitfall.

Design: Tissue microarrays (triplicate 1 mm cores) were constructed from all mesotheliomas in our files from 1975-2018 for which a block was available and the diagnosis could be confirmed. Polyclonal PAX8 immunohistochemistry was assessed for intensity (0-3+) and extent (0-100%) with an H-score calculated (intensity*extent). Fisher's exact and Mann-Whitney tests were used with $p<0.05$ considered significant.

Results: The cohort included 88 malignant (59 pleural, 29 peritoneal; 76 epithelioid, 7 biphasic, 5 sarcomatoid), 18 benign multicystic peritoneal, and 3 well-differentiated papillary mesotheliomas. PAX8-positivity was more frequent in peritoneal (31%) than pleural (12%) malignant mesothelioma ($p=0.004$) and was more common in women (30%) than men (10%) in malignant mesothelioma. It was most common in benign multicystic peritoneal mesothelioma (61%; $p=0.0004$ vs all other cases). Median H-scores were not significantly different for these comparisons. Forty-five (45) percent of peritoneal mesotheliomas in women were PAX8-positive (mean/median H-score 69/33). Detailed data are presented in the Table.

	n	Mean (Median) Age	Gender	% PAX8+	Mean (Median) H-score (if positive)
Malignant mesothelioma (all)	88	58 (60)	51M:37W	18%	81 (28)
Malignant mesothelioma (pleural)	59	64 (64)	42M:17W	12%	95 (17)
Malignant mesothelioma (peritoneal)	29	47 (47)	9M:20W	31%	69 (33)
Malignant mesothelioma (epithelioid)	76	56 (57)	41M:35W	20%	85 (33)
Malignant mesothelioma (sarcomatoid)	5	73 (73)	4M:1W	0%	NA
Malignant mesothelioma (biphasic)	7	69 (66)	6M:1W	14%	10 (10)
Malignant mesothelioma (men)	51	63 (63)	NA	10%	19 (15)
Malignant mesothelioma (women)	37	52 (54)	NA	30%	108 (43)
Benign multicystic mesothelioma	18	43 (54)	2M:16W	61%	49 (40)
Well-differentiated papillary mesothelioma	3	60 (57)	1M:2W	0%	NA

Conclusions: Our study highlights frequent PAX8-positivity in mesothelial proliferations, especially in women, in the peritoneum, and, particularly, in benign multicystic peritoneal mesothelioma, which must be kept in mind when PAX8 is used as part of a panel to distinguish Müllerian and mesothelial lesions. Occasional PAX8-positivity is also seen in the pleura and in men, which could lead to a misdiagnosis of renal cell carcinoma in the unaware.

851 Comparison of the Spectrum and Frequency of Solid Tumors with NRG1 Gene Fusion in European and the USA Population

Ondrej Ondic[1], Nikola Ptakova[2], Reza Alaghehbandan[3]
[1]Biopticka laborator s.r.o., Pilsen, Czech Republic, [2]Molecular and Genetic Laboratory, Biopticka Lab, Ltd, Plzen, Czech Republic, [3]Royal Columbian Hospital, University of British Columbia, New Westminster, BC

Disclosures: Ondrej Ondic: None; Nikola Ptakova: None; Reza Alaghehbandan: None

Background: The newly described fusion genes containing Neuregulin-1 (NRG1) are newly described potentially actionable oncogenic drivers. NRG1 containing fusion genes promote pathologic signaling via major described canonical pathways. In vitro studies have shown targeting ERRB2 and ERRB3 in such tumors may be an effective treatment strategy. Initial clinical trials have shown a positive response to this treatment in some cases of lung adenocarcinoma, cholangiocarcinoma, and pancreatic ductal adenocarcinoma. Effective large scale identification of tumors harboring this rare gene fusion is an open question. We present our experience with NRG1 fusion gene tumors identified retrospectively in our tumor registry based on molecular profiling of 3262 tumors.

Design: This is a retrospective study examining the deidentified molecular profiling database of 3262 solid tumors submitted for a fusion testing to reference laboratory in the Czech Republic from tertiary care hospital routine biopsy as well as consult cases during 2016-2019. Gene fusion detection was performed using the Archer Fusion Plex kits for Illumina (ArcherDX Inc., Boulder, CO). The resulting FASTQ files were analyzed using the Archer Analysis software (ArcherDX Inc.).

Results: The sample population consisted of 3262 unique tumors. The frequency of tumors with NRG1 gene fusion in the entire tested population was 0.18 % (6/3262). The most common histologic type was lung adenocarcinoma (n=4), followed by renal cell carcinoma (n=1), and prostatic adenocarcinoma (n=1). Identified fusion partners were of wide range (CD74, TNC, VAMP2, UNC5) including recurring one - SDC4. There were no co-occurrences with other tested fusion or gene mutation.

The overall frequency of tumors with NRG1 fusion in our study (0.18%) is comparable to that being reported in the literature.
We also confirm that lung adenocarcinoma is the most frequent tumor presenting NRG1 fusion.
The spectrum of tumors cannot be fully compared due to a low number of cases identified.
Frequency of tumors harboring NRG1 fusion in the tested European population equals the USA tested population.

852 MicroRNA-Based Classification of Neuroendocrine Neoplasms

Kaitlin Vanderbeck[1], Jina Nanayakkara[2], Kathrin Tyryshkin[2], Justin Wong[2], Xiaojing Yang[2], Paula Ginter[3], Theresa Scognamiglio[3], Neil Renwick[4]
[1]Queen's University/Kingston Health Sciences Centre, Kingston, ON, [2]Queen's University, Kingston, ON, [3]Weill Cornell Medicine, New York, NY, [4]Kingston General Hospital, Queen's University, Kingston, ON

Disclosures: Kaitlin Vanderbeck: None; Jina Nanayakkara: None; Kathrin Tyryshkin: None; Justin Wong: None; Xiaojing Yang: None; Paula Ginter: None; Theresa Scognamiglio: None; Neil Renwick: None

Background: Neuroendocrine neoplasms (NENs) are clinically diverse tumors that affect multiple organs and lack a single defining molecular marker. MicroRNAs (miRNAs) are small RNA molecules that are excellent biomarkers due to their stability, abundance, cell-type and disease-stage specificity. To date, there are no comprehensive miRNA profiling studies characterizing the multiple NEN pathological types affecting different organs and tissues throughout the body. Given their utility in cancer classification, we hypothesized that miRNAs can be used to define and classify NENs of different organ sites.

Design: Comprehensive miRNA expression profiles for 221 fresh and formalin-fixed paraffin embedded (FFPE) NEN tissue samples, representing 15 different pathological types, and 114 non-NEN controls were generated through barcoded small RNA sequencing. Specifically, NENs from the skin, thyroid gland, parathyroid glands, adrenal glands, pituitary gland, lung, pancreas and gastrointestinal tract were included. Following data quality control, we compared miRNA expression in NEN and non-NEN samples through high expression analyses and built a hierarchical machine-learning model for NEN classification.

Results: We found that miR-375 was abundantly expressed in all NENs and significantly higher in NEN compared to non-NEN tissues. Within NENs, machine learning models identified 17 miRNAs that could accurately discriminate all 15 pathological types. These miRNAs

were subsequently used in a multi-layer machine-learning model that separates NENs on developmental (epithelium vs. neuroectoderm) and anatomic origin, with 97-100% accuracy at each layer of the classifier.

Conclusions: We provide compelling evidence that miR-375 is a universal mono-analyte marker of NEN tissue differentiation. We also show that NENs can be accurately classified through high quality miRNA expression profiling and machine-learning models. Our findings could be used to improve NEN detection as well as advance our knowledge of neuroendocrine tumorigenesis.

853 Comparison of Immunohistochemistry to a Clinicopathologic Classifier in the Diagnosis of Primary Mucinous Ovarian Tumor

Neha Varshney[1], Ilham Farhat[2], Andrew Bellizzi[2]
[1]The University of Arizona, Tucson, AZ, [2]University of Iowa Hospitals and Clinics, Iowa City, IA

Disclosures: Neha Varshney: None; Ilham Farhat: None; Andrew Bellizzi: None

Background: Ovarian involvement by non-Müllerian mucinous epithelial tumors (i.e., low-grade appendiceal mucinous neoplasm or metastatic carcinoma) is frequently mistaken for a primary mucinous ovarian tumor. We routinely employ a clinicopathologic classifier originally published by Yemelyanova (PMID: 18162780) and immunohistochemistry (IHC) in this setting. We undertook this study, at least in part, given availability of a newly validated pan-gastrointestinal marker (CDH17) and monoclonal PAX8 in our laboratory.

Design: IHC for CK7, CK20, CDX2, PAX8 (rabbit monoclonal EP298), SATB2, and CDH17 was performed on tissue microarrays of 101 primary mucinous ovarian tumors (33 carcinomas, 41 borderline tumors, 27 cystadenomas). Markers were assessed for intensity (0-3+) and extent (0-100%) of expression with an H-score calculated (intensity*extent). Patient age, tumor size (cm), and presence of uni- or bilateral tumor was recorded. For the clinicopathologic classifier, bilateral tumors and unilateral tumors <13 cm are designated metastatic; for the IHC classifier, cases with any PAX8-positivity are designated primary, PAX8-negative tumors with CK20 and/or CDX2 H-scores ≥200 are designated metastatic, and all others are deferred.

Results: Detailed data are presented in the Table.

CDH17 was frequently, strongly expressed across all three tumor classes (44%; mean/median H-score 164/175); SATB2 was only expressed by 2 tumors (H-scores 230, 300), both of which arose in association with a mature cystic teratoma; somewhat surprisingly, PAX8 was frequently, strongly expressed (73%; mean/median H-score 206/240).

Although the IHC classifier was only marginally more frequently correct than the clinicopathologic classifier (70% vs 62%), it was very rarely incorrect (4%, while it deferred in 26%).

	Carcinoma	Borderline	Cystadenoma
Age Mean (Median)	57 (57)	51 (55)	51 (52)
Unilateral/Bilateral	U: 82% B: 18%	U: 93% B: 7%	U: 81% B: 19%
Size (cm) Mean (Median)	19 (17)	19 (20)	15 (13)
CK7 % Positive Mean (Median) H-score	97% 215 (265)	97% 238 (245)	100% 260 (285)
CK20 % Positive Mean (Median) H-score	48% 77 (60)	51% 103 (65)	7% 75 (30)
CDX2 % Positive Mean (Median) H-score	39% 51 (15)	35% 88 (49)	11% 98 (35)
PAX8 % Positive Mean (Median) H-score	75% 202 (260)	85% 196 (200)	54% 238 (275)
CDH17 % Positive Mean (Median) H-score	52% 168 (175)	49% 159 (175)	27% 166 (170)
Clinicopathologic Classifier (Primary/Metastatic)	P: 64% M: 36%	P: 71% M: 29%	P: 48% M: 52%
IHC Classifier (Primary/Metastatic/Defer)	P: 73% M: 0% D: 27%	P: 80% M: 7% D: 12%	P: 52% M: 4% D: 44%

Conclusions: This study affirms our combined clinicopathologic and IHC approach to tumors in the ovary with mucinous histology. Unlike SATB2 (which is only strongly positive in rare primary tumors arising in a teratoma), CDH17 has no value in this setting. Frequent (75%), strong PAX8-positivity in primary mucinous ovarian tumors far exceeds the rate in the aggregated published literature (30%), possibly attributable to use of a monoclonal antibody.

854 Liver Metastases from Pituitary Carcinoma Mimicking Visceral Well-Differentiated Neuroendocrine Tumor

Elise Venable[1], M. Beatriz Lopes[2], Andrew Bellizzi[3], Aditya Raghunathan[1], Karra Jones[4], Thorvardur Halfdanarson[1], Sarah Kerr[5], Oksana Hamidi[6], Mabel Ryder[1], Taofic Mounajjed[1], Rondell Graham[1]
[1]Mayo Clinic, Rochester, MN, [2]University of Virginia Health System, Charlottesville, VA, [3]University of Iowa Hospitals and Clinics, Iowa City, IA, [4]The University of Iowa, Iowa City, IA, [5]Hospital Pathology Associates, PA, Minneapolis, MN, [6]University of Texas Southwestern, Dallas, TX

Disclosures: Elise Venable: None; M. Beatriz Lopes: None; Andrew Bellizzi: None; Aditya Raghunathan: None; Karra Jones: *Consultant*, Audentes Therapeutics; Thorvardur Halfdanarson: None; Sarah Kerr: None; Oksana Hamidi: None; Mabel Ryder: None; Taofic Mounajjed: None; Rondell Graham: None

Background: Neuroendocrine neoplasms presenting as metastasis to various organs are common in routine surgical pathology practices. These neoplasms are typically well-differentiated tumors with characteristic histologic features. With less frequency, there are cases of metastatic pituitary carcinoma presenting in the liver simulating well-differentiated neuroendocrine tumors. Due to rarity of pituitary carcinoma, studies of natural history and pathologic characterization are limited and this entity remains an important differential in the diagnosis of neuroendocrine tumors. The aim of this study was to describe the clinicopathologic features of a series of pituitary carcinomas involving the liver and mimicking histologically well differentiated neuroendocrine tumors of visceral origin.

Design: We identified and retrieved four cases of pituitary carcinoma metastatic to the liver to examine clinical characteristics, histomorphology, immunophenotype, and follow-up. Each case was evaluated using antibodies to chromogranin, CDX2, TTF-1, Islet-1, Ki-67, INSM-1, OSCAR, and T-PIT. We selected a group of well-differentiated neuroendocrine tumors of the pancreas to use as immunophenotypic controls.

Results: We identified four cases of pituitary carcinoma metastatic to the liver from patients aged 51 to 73 (3 female; 1 male). Three of the patients presented with Cushing syndrome and all cases histologically resembled well-differentiated neuroendocrine tumors of visceral origin with Ki-67 proliferation indices of 5-42% and expression of T-PIT; metastatic tumors were not immunoreactive with CDX2, Islet 1 or TTF-1.

Table 1: Summary of the clinical characteristics of the patients with pituitary carcinomas presenting as multiple liver masses

Name	Age at time of liver diagnosis	Interval between pituitary diagnosis and liver diagnosis (months)	Sex	Abdominal imaging findings	8am Serum ACTH (pg/ml)	Status at follow up	Duration of follow up (months)
1	51	16	F	Multiple liver masses	78336	Alive with disease	24
2	65	72	F	Multiple liver masses	33000	Died of disease	86
3	73	52	M	Multiple liver masses	1056	Alive with disease	60
4	50	36	F	Multiple liver masses	unknown	Alive with disease	36

Figure 1 - 854

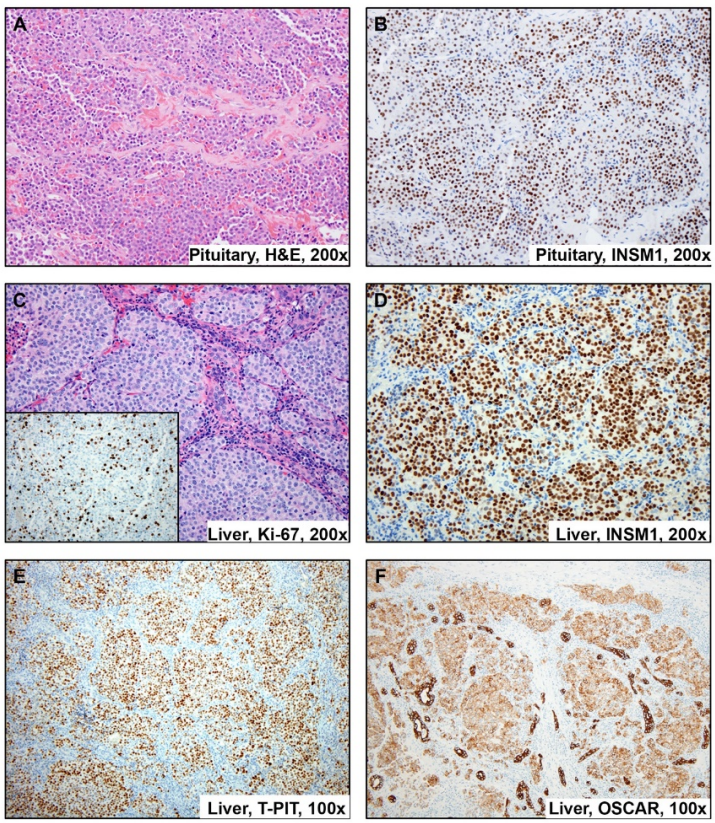

Conclusions: Metastatic pituitary carcinoma is a rare entity with typical histopathological features of a well-differentiated neuroendocrine tumor. These cases commonly have increased adrenocorticotropic hormone (ACTH) secretion and clinical symptomatology of Cushing syndrome. The immunophenotype of these cases are specific for pituitary origin and reacts with pituitary specific transcription factor immunohistochemistry such as T-PIT. While this is an uncommon entity and infrequently encountered diagnosis, the differential diagnosis of pituitary carcinoma should be considered in metastatic histologic well-differentiated neuroendocrine tumors in which the assignment of site of origin is uncertain.

855 INSM1 Expression in Clear Cell Sarcoma of Kidney and other BCOR-Rearranged Tumors

Hannah Wang[1], Erna Forgo[1], Michael Clay[2], Alyaa Al-Ibraheemi[3], Gregory Charville[1]
[1]Stanford University School of Medicine, Stanford, CA, [2]St. Jude Children's Research Hospital, Memphis, TN, [3]Boston Children's Hospital, Boston, MA

Disclosures: Hannah Wang: None; Erna Forgo: None; Michael Clay: None; Gregory Charville: None

Background: Clear cell sarcoma of the kidney (CCSK) is a rare pediatric renal malignancy with variable morphology. Recent studies have demonstrated that more than 80% of CCSKs harbor *BCOR* internal tandem duplications (ITD), and that CCSKs demonstrate upregulated expression of neural markers. We hypothesized that insulinoma-associated protein 1 (INSM1), a transcription factor that functions in neuroepithelial tissue development, would be expressed in CCSK. We additionally hypothesized that INSM1 expression in CCSK could be related to alterations in *BCOR* and might be seen in other *BCOR*-rearranged malignancies.

Design: We evaluated INSM1 expression in 22 CCSKs (8 by whole slide, 14 by tissue microarray), along with 4 *BCOR-CCNB3* sarcomas, 2 high-grade endometrial stromal sarcomas, and 1 high-grade neuroepithelial tumor with *BCOR* alteration. Additionally evaluated were 24 Wilms tumors (11 by whole slide, 13 by tissue microarray), 3 congenital mesoblastic nephromas, 2 malignant rhabdoid tumors, and 4 synovial sarcomas. Immunohistochemical studies for INSM1 (clone A-8) were scored for percentage of neoplastic cells with nuclear expression (0-100%) and maximum intensity of expression (0-3+). Samples were considered positive for INSM1 if 1% or more of cells had expression of any intensity. Immunohistochemistry for synaptophysin and chromogranin was performed on CCSKs.

Results: Altogether, 77% (17/22) of CCSKs were positive for INSM1, all of which demonstrated diffuse weak-moderate expression (Figure 1a-b). In contrast, 33% (8/24) of Wilms tumors were positive for INSM1, all with a focal and strong expression pattern (Figure 1c-d). Focal

INSM1 expression was also seen in a subset of other CCSK morphologic mimics (Table 1). All CCSKs were negative for synaptophysin and chromogranin. Our analysis of published microarray gene expression data (GSE34800) revealed significantly increased INSM1 expression in *BCOR-CCNB3* sarcomas as compared to Ewing sarcoma controls (Figure 2). Overall, *BCOR*-rearranged tumors were significantly more likely to express INSM1 than non-*BCOR*-altered tumors (79% vs. 29%, $p < 0.01$).

Tumor Subtype	INSM1	Degree Positivity#	Intensity^
BCOR-altered tumors	22/28 (79%)	83% (65%-90%)	1-3+
CCSK*	17/22 (77%)	90% (80%-90%)	1-2+
BCOR-CCNB3 fusion sarcoma	3/4	30% (5%-40%)	1-2+
HG-ESS with ZC3H7B-BCOR	1/1	70%	2+
HGNET with BCOR alteration	1/1	5%	3+
Tumors without BCOR alteration	10/34 (29%)	5% (2%-10%)	1-3+
Wilms tumor	8/24 (33%)	4% (1%-9%)	2-3+
Congenital mesoblastic nephroma	1/3	5%	1+
Malignant rhabdoid tumor	1/2	10%	1+
HG-ESS with YWHAE 17p13.3	0/1	-	-
Synovial sarcoma (monophasic)	0/4	-	-

Abbreviations: CCSK – clear cell sarcoma of kidney, HG-ESS – high grade endometrial stromal sarcoma, HGNET – high grade neuroepithelial tumor

* All 5/5 CCSKs with molecular confirmation of BCOR ITD were INSM1 positive

Percentage of nuclei with INSM1 expression of any intensity, reported as median (interquartile range), among all cases positive for INSM1

^ Range of nuclear expression intensity among all cases positive for INSM1

Figure 1 - 855

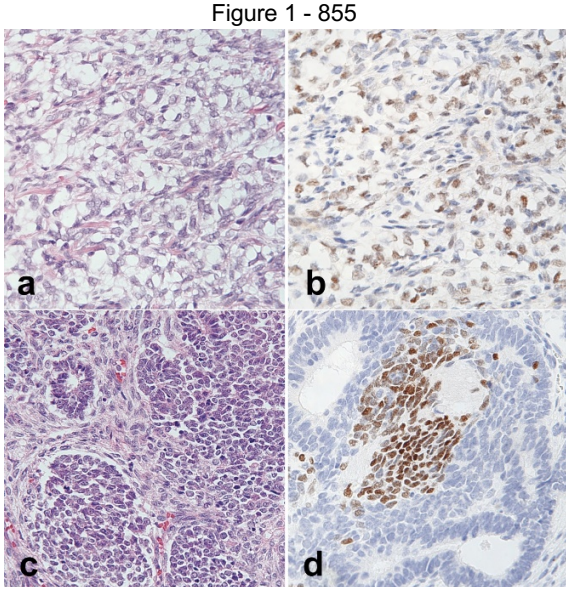

Figure 2 - 855

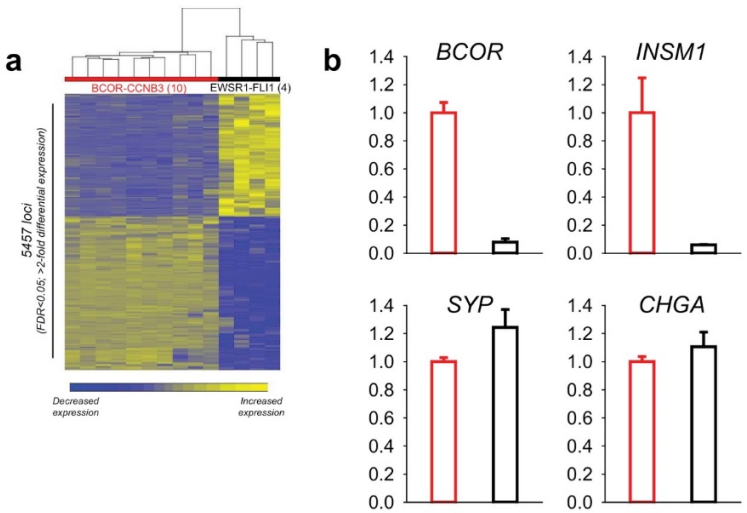

Conclusions: Diffuse weak-moderate INSM1 expression was unique to CCSK among evaluated mimics. INSM1 expression was also seen in a subset of other *BCOR*-altered tumors. Identification of INSM1 expression may aid in the classification of certain neoplasms bearing *BCOR* gene rearrangements, including CCSK; recognition of INSM1 expression as a feature of these tumors may help to avoid a diagnostic pitfall.

856 Widely Divergent Rates of GATA3 Positivity in Chordoma Highlight the Significant Impact of Immunohistochemistry Technique

Jing Yang[1], Samantha Champion[2], Andrew Bellizzi[3], G. Pétur Nielsen[4], Jason Hornick[5]
[1]Brigham and Women's Hospital, Harvard Medical School, Belmont, MA, [2]Massachusetts General Hospital, Boston, MA, [3]University of Iowa Hospitals and Clinics, Iowa City, IA, [4]Harvard Medical School, Boston, MA, [5]Brigham and Women's Hospital, Harvard Medical School, Boston, MA

Disclosures: Jing Yang: None; Samantha Champion: None; Andrew Bellizzi: None; G. Pétur Nielsen: None; Jason Hornick: *Consultant*, Eli Lilly; *Consultant*, Epizyme

Background: Chordoma is a locally aggressive malignant bone tumor that typically occurs in the axial skeleton. Chordoma can sometimes be confused with metastatic adenocarcinoma, given the characteristic strong expression of keratins and EMA. GATA3 is a widely used marker for evaluating carcinomas of unknown primary by immunohistochemistry (IHC); positive results support breast or bladder origin. One of the authors of this study recently encountered a GATA3-positive chordoma that was initially misinterpreted as metastatic urothelial carcinoma and has subsequently noted additional chordoma cases that showed strong GATA3 staining; these findings were not reproduced by another laboratory using a different IHC platform. The objective of this study was to assess IHC for GATA3 in a large cohort of chordoma cases using different detection systems.

Design: A total of 55 chordoma cases were retrieved from the pathology archives of three academic medical centers. All cases were positive for brachyury. IHC was performed following pressure cooker epitope retrieval using a mouse anti-GATA3 monoclonal antibody (1:400 dilution; clone L50-823, Biocare). Appropriate positive controls (breast carcinoma) and negative controls (prostate carcinoma) were used. Two different detection systems were employed: EnVision+ Kit (Agilent Dako) and Novolink Polymer Detection System (Leica). Nuclear staining was scored semiquantitatively for extent and intensity; the results were reported using the H-score.

Results: In total, 22 of 55 (40%) chordoma cases were positive for GATA3 using Novolink; the H-score ranged from 5 to 150 (median H-score 20) (Figure 1). GATA3 staining was not detected using EnVision+, except for one case with an H-score of 1.

Figure 1 - 856

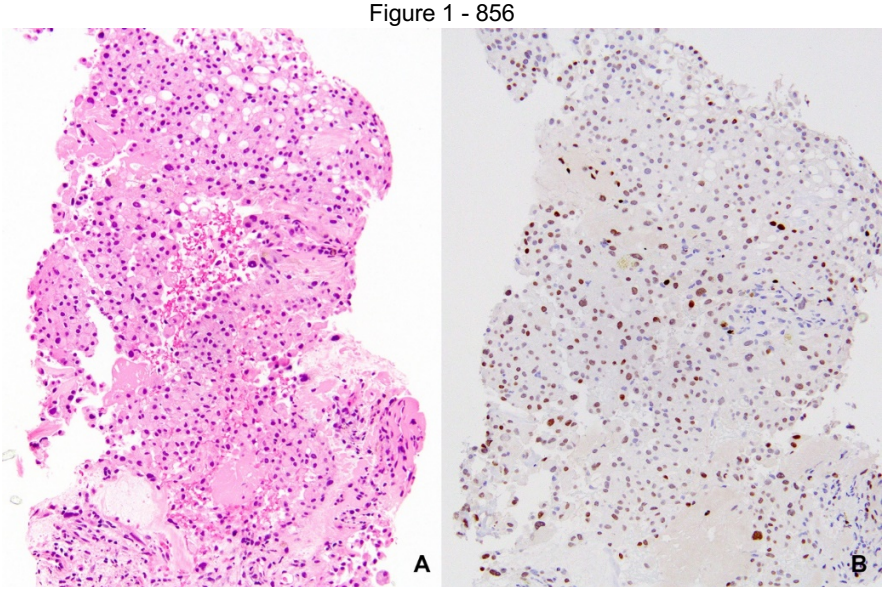

Conclusions: GATA3 is often positive in chordoma using the Novolink detection system (but not EnVision+), which could potentially lead to misdiagnosis of chordoma as metastatic urothelial or breast carcinoma. These findings highlight the significant impact of detection systems on IHC results and emphasize the importance of thorough laboratory validation of diagnostic markers on a wide range of tumor types. Technical factors (including detection chemistry) are likely the greatest cause of sometimes widely differing published results regarding the "expression" of lineage-restricted transcription factors. Unexpected or limited staining for transcription factors should be interpreted with caution in the context of an appropriate panel of markers when evaluating a tumor of unknown origin.

857 Determination of Eligibility for Pembrolizumab Treatment: Comparison of Mismatch Repair Deficiency (dMMR) by IHC, Microsatellite Instability-High (MSI-H) Status by PCR, and MMR Gene Mutations (MMRmut) by NGS

Richard Yang[1], Arash Ronaghy[1], Mustafa Abdulrazzaq[1], Galina Feinstein[1], Mark Routbort[1], Scott Kopetz[1], Russell Broaddus[2], Victor Prieto[1], L. Jeffrey Medeiros[1], Rajyalakshmi Luthra[1], Keyur Patel[1]
[1]The University of Texas MD Anderson Cancer Center, Houston, TX, [2]University of North Carolina School of Medicine, Chapel Hill, NC

Disclosures: Richard Yang: None; Arash Ronaghy: None; Mustafa Abdulrazzaq: None; Galina Feinstein: None; Mark Routbort: None; Scott Kopetz: None; Russell Broaddus: None; Victor Prieto: None; L. Jeffrey Medeiros: None; Rajyalakshmi Luthra: None; Keyur Patel: None

Background: Microsatellite instability high status (MSI-H) by PCR or deficient mismatch repair (dMMR) expression by IHC are FDA approved indications for treatment with pembrolizumab. Somatic mutations in mismatch repair genes (MMR), namely *MLH1, PMS2, MSH2, MSH6* (MMRmut), as assessed by next generation sequencing (NGS) is not well characterized compared to dMMR by IHC and MSI testing by PCR. We interrogated the concordance rates of these reported MMR gene mutations from NGS data against IHC and PCR.

Design: We searched our database of 5,177 NGS reports of solid tumors for cases that harbored a somatic mutation in *MLH1, MSH2, MSH6,* and/or *PMS2*. These MMRmut cases were compared against MMR by IHC and MSI by PCR assessment for concordance. Call variants were annotated as either deleterious (i.e. frame shift, nonsense, splice site) or non-deleterious (missense, in-frame in/del) mutations. The cBioPortal website was used to created lollipop diagrams, to show the distribution of these somatic mutations.

Results: Overall 221 of 5,177 reports (4.27%) revealed somatic mutations in MMR genes. Of the 221 cases, 71 (32.1%) were assessed by IHC only, 18 (8.1%) were tested by both, and 5 (1.9%) were assess by PCR only (Table 1). Remaining 127 (57.5%) were not assessed by either. Of the 94 MMRmut cases with MSI-PCR and/or IHC testing, only 36 (38.3%) found either MSI-H or dMMR status. A total of 311 somatic mutations in MMR genes were detected in 221 cases, of which 60 (19.3%) were deleterious and 251 (80.7%) were non-deleterious. Significant correlation was detected between the nature of mutations (deleterious vs non-deleterious) and MSI-H/dMMR status (p-value <0.0001, Fisher's exact test). Cases with deleterious MMR mutations by NGS were more likely to show MSI-H by PCR and/or dMMR by IHC. Additionally, somatic mutation mapping with these genes reveal an even distribution of somatic mutations, without any overwhelming hotspots.

	No. of cases	MSH2	MSH6	MLH1	PMS2	SM-MMR Cases (%)	Deleterious (%)	Only Non-Deleterious (%)
IHC and/or PCR	**All**	71	70	47	57	**221 (100)**	**46 (20.8)**	**175 (79.2)**
Orthogonal Testing Found MSI-H or dMMR	**Found**	16	8	11	4	**36 (16.2)**	**19 (8.59)**	**17 (7.69)**
	Not Found (Missed)	24	22	7	13	**58 (26.2)**	**6 (2.71)**	**52 (23.5)**
Neither assessed	**Neither assessed**	31	40	29	40	**127 (57.5)**	**21 (9.5)**	**106 (48.0)**
Both Assessed	**Total Both Assessed**	9	6	0	4	**18 (8.14)**	**2 (0.9)**	**16 (7.24)**
	Both Normal	5	3	0	2	**9 (4.07)**	1 (0.4)	8 (3.62)
	MSI-H only found	2	1	0	1	**4 (1.81)**	1 (0.4)	3 (1.36)
	dMMR only found	0	0	0	0	**0 (0)**	0 (0)	0 (0)
	Both MSI-H and dMMR found	2	2	0	1	**5 (2.26)**	0 (0)	5 (2.26)
IHC only	**Total IHC only**	29	21	18	13	**71 (32.1)**	**23 (10.4)**	**48 (21.7)**
	Intact	17	16	7	11	**44 (19.9)**	5 (2.26)	39 (17.6)
	Lost any	12	5	11	2	**27 (12.2)**	18 (8.14)	9 (4.07)
MSI only	**Total MSI only**	2	3	0	0	**5 (2.26)**	**0 (0)**	**5 (2.26)**
	MSI-H	0	0	0	0	**0 (0)**	0 (0)	0 (0)
	MSI-L	0	0	0	0	**0 (0)**	0 (0)	0 (0)
	MSS	2	3	0	0	**5 (2.26)**	0 (0)	5 (2.26)
Mutation Type	**Deleterious**	18	12	12	5	**46 (20.8)**		
	Only Non-Deleterious	51	57	35	49	**175 (79.2)**		
	All Non-Deleterious	53	58	35	51	**179 (81.0)**		

Figure 1 - 857

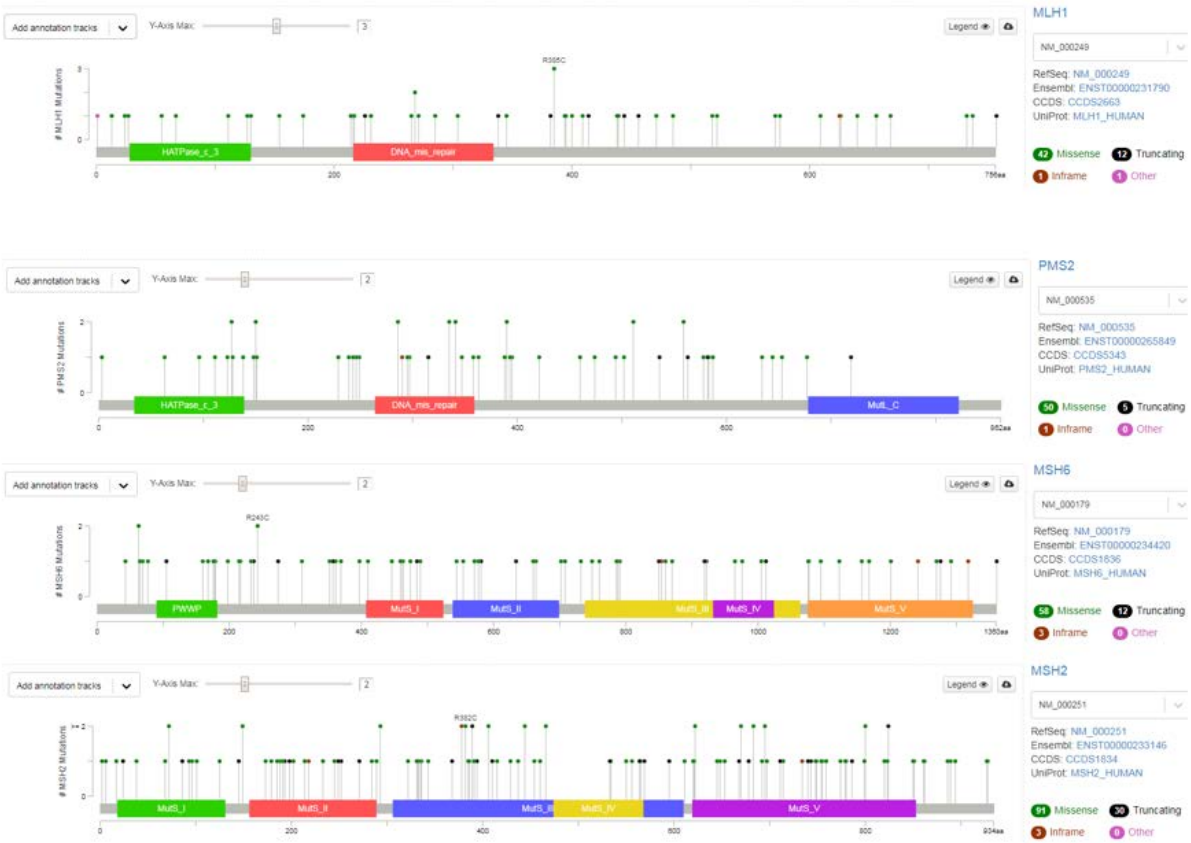

Figure 1. Distribution of somatic mutations in *MLH1, PMS2, MSH2, MSH6* genes using cBioPortal website. These lollipop diagrams show even distribution of these somatic mutations, without any overwhelming hotspots. This would be consistent with a pattern of DNA repair proteins showing loss of function within solid tumors.

Conclusions: MSI PCR and MMR IHC testing assessed only a minority (42.1%) of MMRmut solid tumors. Only a smaller minority of MMRmut tumors (16.2%) were found to be MSI-H or dMMR by conventional methods. Our data shows the frequency and distribution of deleterious versus non-deleterious mutations in MMR genes and helps explain the discordance with MSI-H status by PCR and dMMR by IHC. A larger number of cases tested by all 3 methods needs to be compared to improve our understanding of MSI-H status determination by available laboratory methods.

858 Rapid Slide-Free Pathology Diagnostics Using Full-Color Optical Coherence Microscopy (Full-Color OCM)

Akihiko Yoshizawa[1], Shinji Sumiyoshi[1], Chien-Chung Tsai[2], Hironori Haga[3]
[1]Kyoto University Hospital, Kyoto, Japan, [2]AcuSolutions Inc., Taipei, Taiwan, [3]Kyoto, Japan

Disclosures: Akihiko Yoshizawa: *Primary Investigator*, Acusolutions.inc; Shinji Sumiyoshi: None; Chien-Chung Tsai: None; Hironori Haga: None

Background: Some techniques, which enable visualization of unsectioned blocks or unstained glass slides, have been proposed. Conventional full-field optical coherence microscopy (FF-OCM), which is one of the techniques, is capable of providing cell-level cytoplasmic images without using expensive components; however, it is difficult to visualize nuclei in detail using this technique. Moreover, the technique is not able to create color images. We propose a novel slide-free imaging method using FF-OCM combined with fluorescence (full-color OCM) to make color digital histological images, which can be synthesized into pseudo-hematoxylin-and-eosin (p-H&E) images. This study demonstrates rapid histological imaging of unsectioned surgical or fresh specimens using full-color OCM and assesses its quality compared to conventional H&E staining of formalin-fixed paraffin-embedded (FFPE) tissues.

Design: A total of 106 formalin-fixed surgical specimens and 120 fresh specimens from 11 autopsy cases were collected. After all specimens were scanned by full-color OCM, the corresponding FFPE tissues were processed for making conventional H&E slides and compared to full-color OCM images.

Results: The optical system (Fig. 1) takes about 4 min to scan a 1-cm^2 area and a total of 15 min from receiving the specimen to complete the scan. Full-color OCM enabled the identification of normal histology from various organs, including the skin (Fig. 2A), brain, breast, soft tissue, gastrointestinal tract, salivary gland (Fig. 2B), respiratory system, hepatobiliary system, genitourinary tract, and hematolymphoid system. Moreover, diagnostic results, including pleomorphic adenoma, nodular goiter, liver cirrhosis, leiomyoma (Fig. 2C), meningioma, adenocarcinoma, squamous cell carcinoma, spindle cell sarcoma glioma, testicular seminoma (Fig. 2D), and lymphoma from various organs, were made from p-H&E images, which were created by full-color OCM.

Figure 1 - 858

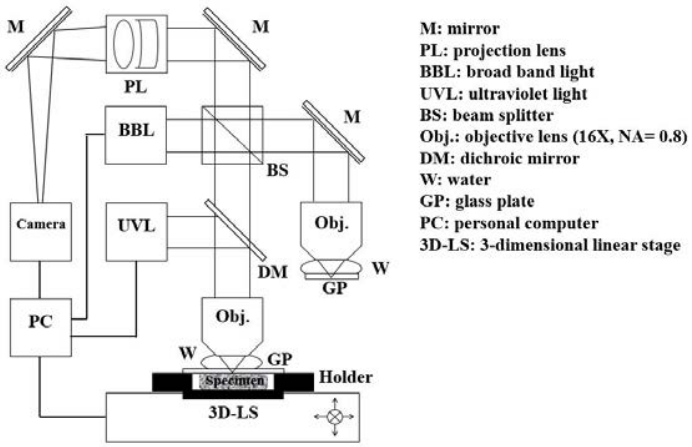

Figure 1. The optical system with full-color optical coherence microscopy (full-color OCM) using a pair of objective lenses, wherein conventional OCM source is broad band light (BBL). Specimen was stained by fluorescent dye and excited by ultraviolet light (UVL).

Figure 2 - 858

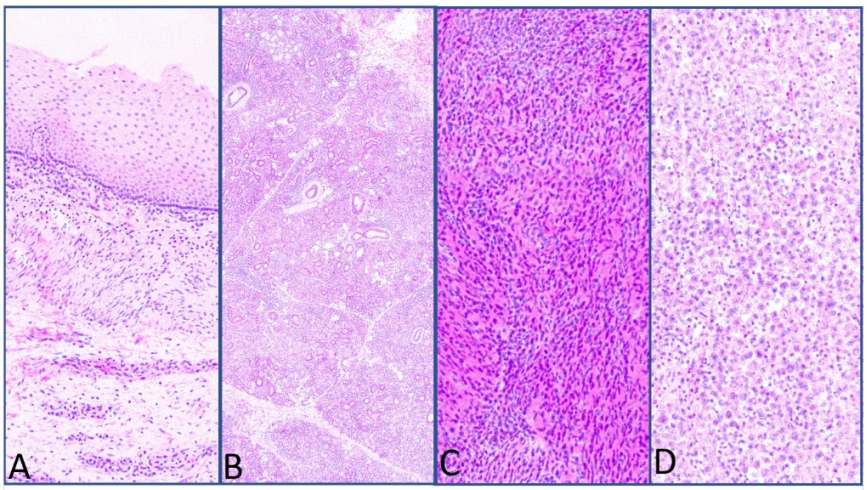

Figure 2. Representative pseudo-hematoxylin-and-eosin (p-H&E) images created by full-color OCM. (A) normal skin from surgical specimen, (B) normal salivary gland from surgical specimen, (C) leiomyoma from fresh specimen, and (D) seminoma from surgical specimen.

Conclusions: Full-color OCM images closely resembled FFPE-H&E images and enabled rapid assessment of normal and pathological histology in both fixed and fresh specimens. This technology has the advantages of fast imaging by skipping sectioning procedures, leading to increased opportunities for intra-operative consultation and saving costs by removing the need to process FFPE tissues. Furthermore, it has the potential to provide a digital pathologic platform for telepathology and rapid artificial intelligence assisted diagnosis.

859 INSM1 is a More Sensitive General Neuroendocrine Marker than Chromogranin A and Synaptophysin in the Diagnosis of Poorly Differentiated Neuroendocrine Carcinoma

Yanmin Zhang[1], Matthew Gosse[2], Andrew Bellizzi[1]
[1]University of Iowa Hospitals and Clinics, Iowa City, IA, [2]Iowa City, IA

Disclosures: Yanmin Zhang: None; Matthew Gosse: None; Andrew Bellizzi: None

Background: Insulinoma-associated protein 1 (INSM1) is gaining traction as a general neuroendocrine marker. We are currently deciding if and how to use it in our practice. We were intrigued by a couple recent reports of increased sensitivity in poorly differentiated neuroendocrine carcinomas (NEC), relative to the traditional neuroendocrine markers chromogranin A (CgA) and synaptophysin (Syn). 10-20% of non-neuroendocrine carcinomas (non-NE CA) express CgA and/or Syn (i.e., so-called "occult neuroendocrine differentiation"), and INSM1 is not well-characterized in this setting.

Design: Immunohistochemistry (IHC) for INSM1 (clone A-8), CgA, and Syn was performed on tissue microarrays of 30 small cell lung cancers (SCLC), 20 extrapulmonary visceral (EPV)-NECs, 43 Merkel cell carcinomas (MCC), and 87 non-NE CAs metastatic to brain, including adenocarcinomas of the lung (36), breast (10), kidney (7), colon (7), and esophagus (5); squamous cell CAs (6); urothelial CAs (5); and other CAs (12). IHC was assessed for intensity (0-3+) and extent (0-100%), and an H-score was calculated (intensity*extent). Fisher's exact and Kruskal-Wallis tests with post tests were used with $p<0.05$ considered significant.

Results: INSM1 was more frequently expressed in NECs (95%) than either CgA (83%) or Syn (82%) ($p=0.03$ and 0.0001); the median INSM1 H-score (240) was greater than that for CgA (150) ($p<0.01$). At an H-score threshold of ≥50 (simulating what we apply clinically; i.e., we typically ignore weak, patchy general neuroendocrine marker staining), INSM1 maintains 88% sensitivity, while that of CgA and Syn drop to 61% and 76%, respectively. INSM1, CgA, and Syn were expressed by 23%, 10%, and 14% of non-NE CAs, each with typically weak, patchy staining (all median H-scores ≤15). At the H-score threshold of ≥50, INSM1 was 88% sensitive and 99% specific for NEC vs non-NE CA. Detailed data are presented in the Table.

	INSM1 % Positive Mean (median) H-score	CgA % Positive Mean (median) H-score	Syn % Positive Mean (median) H-score
SCLC (n=30)	97% 198 (240)	83% 114 (100)	72% 195 (230)
EPV-NEC (n=20)	90% 216 (240)	65% 169 (150)	70% 239 (275)
MCC (n=43)	95% 240 (265)	91% 182 (185)	93% 195 (205)
All NEC (n=93)	95% 222 (240)	83% 158 (150)	82% 203 (240)
Non-NE CA (n=87)	23% 10 (7)	10% 21 (15)	14% 23 (13)

Conclusions: INSM1 is more sensitive than CgA and Syn in the diagnosis of NEC. As with the traditional general neuroendocrine markers, a significant minority of non-NE CAs demonstrate weak, patchy INSM1 expression; this quality of staining should not be taken as evidence of NEC. Given these findings, we have deployed "INSM1 alone" as our first-tier marker to confirm the morphologic impression of NEC.